The Journal of Experimental Biology 214, 131-146

doi:10.1242/jeb.048157

RESEARCH ARTICLE

Mechanics, hydrodynamics and energetics of blue whale lunge feeding: efficiency dependence on krill density

J. A. Goldbogen[1,*], J. Calambokidis[2], E. Oleson[3], J. Potvin[4], N. D. Pyenson[5], G. Schorr[2] and R. E. Shadwick[6]

[1]Scripps Institution of Oceanography, University of California, San Diego, 9500 Gilman Dr., La Jolla, CA 92093-0205, USA, [2]Cascadia Research Collective, 218 W. 4th Ave., Olympia, WA 98501, USA, [3]Pacific Islands Fisheries Science Center, NMFS/NOAA, Honolulu, HI 96822, USA, [4]Department of Physics, Saint Louis University, 3450 Lindell Boulevard, Saint Louis, MO 63103, USA, [5]Department of Paleobiology, National Museum of Natural History, Smithsonian Institution, Washington, DC 20560, USA and [6]Department of Zoology, University of British Columbia, Vancouver, BC, Canada V6T 124

*Author for correspondence (jergold@ucsd.edu)

Accepted 5 October 2010

SUMMARY

Lunge feeding by rorqual whales (Balaenopteridae) is associated with a high energetic cost that decreases diving capacity, thereby limiting access to dense prey patches at depth. Despite this cost, rorquals exhibit high rates of lipid deposition and extremely large maximum body size. To address this paradox, we integrated kinematic data from digital tags with unsteady hydrodynamic models to estimate the energy budget for lunges and foraging dives of blue whales (*Balaenoptera musculus*), the largest rorqual and living mammal. Our analysis suggests that, despite the large amount of mechanical work required to lunge feed, a large amount of prey and, therefore, energy is obtained during engulfment. Furthermore, we suggest that foraging efficiency for blue whales is significantly higher than for other marine mammals by nearly an order of magnitude, but only if lunges target extremely high densities of krill. The high predicted efficiency is attributed to the enhanced engulfment capacity, rapid filter rate and low mass-specific metabolic rate associated with large body size in blue whales. These results highlight the importance of high prey density, regardless of prey patch depth, for efficient bulk filter feeding in baleen whales and may explain some diel changes in foraging behavior in rorqual whales.

Key words: blue whale, diving, drag, energetics, filter feeding, foraging.

INTRODUCTION

Obligate suspension filter feeding occurs across many different lineages of marine vertebrates that demonstrate convergent specializations for processing vast quantities of small prey items from seawater (Sanderson and Wassersug, 1993). This ability to bulk filter feed has been correlated with large body size or large population biomass, with examples of this phenomenon at the individual level including some of the largest known cetaceans and bony fishes (Alexander, 1998; Friedman et al., 2010). The transfer of mass from prey to predator on such a scale suggests that bulk filter feeding is energetically efficient. Furthermore, this method allows filter feeders to exploit lower trophic levels of the food web, thereby reaping the benefits of greater biomass and energy (Werth, 2000). Cetaceans provide an especially useful comparative context for illustrating this phenomenon: it is generally assumed that the larger average body size of baleen whales (Mysticeti) relative to toothed whales (Odontoceti) directly reflects the greater efficiency of bulk filtration compared to hunting single prey items (Williams, 2006). This assumption, however, remains untested and the effects of body size and feeding mode on the energetics of foraging in cetaceans remain poorly understood.

The two largest living mysticetes, blue (*Balaenoptera musculus*) and fin whales (*B. physalus*), represent the largest living animals, reaching maximum lengths of ~30 m and with a mass that well exceeds 100,000 kg (Mackintosh and Wheeler, 1929). The early ontogenetic stages of these large rorqual whales, particularly the prenatal and pre-weaning periods, are characterized by rapid growth that is fueled by the energetic investment from the mother (Lockyer, 2007). The high rate of lipid deposition that occurs during summer feeding bouts not only facilitates fetal and neonatal growth, but it is also essential for fasting and long-distance migration between foraging and breeding grounds (Brodie, 1975). Coupled with the metabolic consequences of a carnivorous and fully aquatic lifestyle (Williams et al., 2001), these energetic requirements represent a significant foraging demand and require an efficient feeding mechanism.

Balaenopterids feed in bulk by intermittently engulfing large volumes of water that contain dense aggregations of plankton or nekton. This lunge feeding behavior occurs anywhere prey is particularly dense and abundant, from the sea surface (Friedlaender et al., 2009) to more than 500 m in depth (Panigada et al., 1999). During a single lunge, rorquals accelerate to high speed towards a prey patch (Friedlaender et al., 2009; Goldbogen et al., 2008; Goldbogen et al., 2006) and open their mouths wide to approximately 80 deg (Brodie, 1993; Brodie, 2001). The dynamic pressure generated by an open mouth at high speed causes the inflation of the buccal cavity (Goldbogen et al., 2007), whereby the tongue inverts and forms a large portion of the capacious sac that envelopes the engulfed water mass (Lambertsen, 1983). The enhanced capacity of the buccal cavity is also facilitated by a specialized blubber layer, the ventral groove blubber (VGB), which spans 50–60% of the whale's body length from the anterior of the

snout to the umbilicus (Goldbogen et al., 2010). The VGB is an accordion-like blubber layer that is compact and held against the body during steady swimming, conforming to the highly streamlined body profile that is representative of rorquals (Williamson, 1972). Upon death, the VGB unfolds with the loss underlying muscle tone (Goldbogen, 2010), and, in some cases of advanced decomposition, it will expand as the cavum ventrale (an intermuscular cleft between the VGB and the body wall) inflates with pressurized gas. The mechanical properties of the VGB confirm this highly elastic tissue property, demonstrating reversible extensibility up to several times its post-mortem resting length (Orton and Brodie, 1987).

Based on these mechanical properties and a simple hydrostatic model representing the buccal cavity as a thin-walled cylinder, previous researchers have suggested an entirely passive engulfment process whereby the compliance of the buccal cavity is met with little resistance to oncoming flow (Lambertsen, 1983; Orton and Brodie, 1987). However, unsteady hydrodynamic models suggest that the inflation of the buccal cavity is resisted by eccentric contraction of the muscles that adjoin tightly to the VGB (Potvin et al., 2009). Under this scenario, the engulfed water is gradually accelerated forward by virtue of action–reaction (Potvin et al., 2009), and a forward 'push' of the engulfed water mass gives rise to a novel source of hydrodynamic drag from inside the mouth (engulfment drag), in addition to the drag generated from flow around the body (shape drag). The combined drag acting on the whale's body rapidly dissipates its kinetic energy, bringing the lunging whale to a near halt. After mouth closure, the buccal cavity is depressed and the engulfed water is filtered through the baleen racks, thereby leaving captured prey inside the mouth. During this purging phase, rorquals exhibit relatively low speeds and generally adopt a gliding locomotor strategy, as the engulfed water is filtered at a rate of several cubic meters per second (Goldbogen et al., 2007). When the engulfed water is completely filtered, the subsequent lunge requires acceleration from a much lower initial speed.

Because of the high drag required for engulfment and the acceleration of the engulfed water mass, lunge feeding is thought to incur a high energetic cost (Goldbogen et al., 2007; Potvin et al., 2009). This cost has a significant impact on rorqual foraging ecology by limiting their diving capacity (Acevedo-Gutierrez et al., 2002; Croll et al., 2001) and, therefore, restricting access to prey in both space and time. Despite this cost, however, it is hypothesized that lunge feeding is energetically efficient because the large volume of water that is engulfed provides a large amount of ingested prey (Goldbogen et al., 2007; Potvin et al., 2009). Although the basic mechanics of lunge feeding are relatively well understood, reconciling the aforementioned contrasting hypotheses requires investigation of the detailed energetics of rorqual feeding. Here we present a kinematic analysis of blue whale lunge feeding based on data obtained from high-resolution acoustic tags. These data were then incorporated into previously published hydrodynamic models of engulfment in order to gain more insight into the energetics of lunge-feeding rorquals.

MATERIALS AND METHODS

Tag data

We deployed suction cup archival data loggers (Bioacoustic probe, Greenridge Sciences, Goleta, CA, USA) to the backs of surfacing blue whales (*B. musculus* Linnaeus 1758) off the coast of California and Mexico, in the eastern North Pacific Ocean. Sensors within the tag included a pressure transducer, a two-axis accelerometer and a hydrophone. The pressure and accelerometer data were sampled at 1 Hz whereas the hydrophone sampled at 1025 Hz. The data recorded by the tag allowed us to determine dive depth, swimming speed, body orientation (i.e. body pitch) and bouts of active swimming strokes (Goldbogen et al., 2008; Goldbogen et al., 2006). We used high and low pass filters at 0.1 Hz to separate out high (i.e. swimming strokes) and low frequency (i.e. depth, body pitch) signals, respectively. We used the flow noise method, where the tag was towed in water at known speeds to determine the relationship between the flow noise recorded by the tag and the ambient flow speed. This relationship was then used to estimate the speed of the whale from the level of flow noise detected by the tag. In some instances, such as very steep lunges, we were able to compare the speed calculated from flow noise to the speed estimated from the kinematics of the body (vertical velocity divided by the sine of the body pitch angle).

The speed profiles were primarily used in hydrodynamic modeling (see below), but we also used these data to determine the time spent during pre-engulfment acceleration and the time required to filter the engulfed mass (the time between consecutive lunges at depth). Speed profiles for each lunge were superimposed on top of one another and synchronized with respect to maximum speed for comparison. These data were amassed within each tagged whale and then averaged across all individuals to determine the variance in lunge speed.

Morphological data

To estimate engulfment volume and energetic expenditures during lunge feeding, we collected morphological information specific to the engulfment apparatus. These data were derived mainly from linear measurements of the skull and with associated mandibles. We obtained these morphometric data from blue whale specimens reposited at the National Museum of Natural History in Washington, DC (USNM 124326), the Santa Barbara Natural History Museum (SBNH 2447), the Los Angeles County Museum (LACM 72562) and the Long Marine Laboratory at the University of California, Santa Cruz (LML GOGA 1982). Other morphological measurements, including the length of the ventral groove system, body girth, body mass and other dimensions of the engulfment apparatus, were obtained from previous studies (Goldbogen et al., 2010; Lockyer, 1976; Mackintosh and Wheeler, 1929). All morphological variables were recorded as a function of total body length, from the tip of the snout to the notch of the flukes, in order to parameterize the hydrodynamic and bioenergetic models for different sizes of blue whales.

Energy expenditure and engulfment volume during lunge feeding

We estimated the energetic cost of lunge feeding using an unsteady hydrodynamic model (Potvin et al., 2009; Potvin et al., 2010), which predicts the trajectory of both the lunging whale and the engulfed water mass (Appendices 1 and 2). Speed profiles predicted by the model were compared to the empirical speed data from the tags in order obtain the most realistic lunge-feeding simulations. The model incorporated kinematic data from the digital tags and morphological data of the engulfment apparatus to simulate the forces at play during a lunge. The magnitude and duration of these forces allowed us to calculate the mechanical energy required for engulfment. The mechanical energy required for the acceleration phase prior to engulfment was assumed to be approximately two-thirds of the mechanical energy expended during engulfment (Potvin et al., 2009). For all calculations in this study, mechanical energy was converted to metabolic energy using an efficiency of 0.25 (Ahlborn, 2004; Fish and Rohr, 1999) and a propulsive efficiency

of 0.90 (Bose and Lien, 1989), as illustrated in the calculation example shown in Fig. A1. Specifically, metabolic efficiency here represents a 75% bulk loss owing to a variety of factors (i.e. muscle efficiency). Propulsive efficiency assumes a 10% loss of energy when producing thrust. Collectively, we assumed an 85% loss, or a combined efficiency of 0.15. These values are unknown in cetaceans, so we chose 0.15 as a conservative estimate.

Maximum engulfment capacity and, therefore, the magnitude of the engulfed mass were estimated from the dimensions of the skull, mandibles and ventral groove system (Goldbogen et al., 2010; Goldbogen et al., 2007). Trajectory simulations of active engulfment, where the engulfed water mass is slowly accelerated forward over the course of the lunge, were modified to match the speed profile generated by the digital tag data (Potvin et al., 2009). Successful simulations required that the magnitude of the engulfed mass was maximized at the moment of mouth closure. The gape angle dynamics predicted by the model were corroborated by kinematic data obtained from helicopter video of lunge feeding in blue whales at the sea surface (N=5; courtesy of Earl Richmond at Richmond Productions). We ran a total of 20 engulfment simulations for three different blue whale sizes: 22, 25 and 27 m in length. Lunges were simulated at different maximum speeds and different drag coefficients (Potvin et al., 2009) to assess the overall sensitivity of the model to input parameters (note: the engulfment simulations were also compared with simple but well-motivated 'veracity' checks, as described in Appendix 1).

Energy expenditure during diving

The energetic costs of diving were assumed to be equal to field (or active) metabolic rate (FMR or AMR, respectively). We used a mean estimated from three independent allometric metabolic rate models (Croll et al., 2006) to account for all maintenance (i.e. heat increment of feeding) and swimming costs (related to steady-state drag) that occur during diving (including purging and filtering of engulfed water in between lunges), as well as during surface recovery time between foraging dives (see example in Fig. A1). The allometric equations given by Croll et al. (Croll et al., 2006) are as follows:

$$\mathrm{AMR}^{1}(\mathrm{W}) = 12.3M^{\mathrm{body}0.75}, \quad (1)$$

$$\mathrm{AMR}^{2}(\mathrm{W}) = 9.84M^{\mathrm{body}0.756}, \quad (2)$$

$$\mathrm{FMR}(\mathrm{W}) = 8.88M^{\mathrm{body}0.734}, \quad (3)$$

where W is watts and M^{body} is mass in kg.

Although the power required for different phases of a dive are likely to change, it has been shown that the metabolic savings that occur during passive gliding on descent are generally proportional to the additional energetic costs of active swimming during ascent (Fahlman et al., 2008b).

This approximation of energy expenditure probably overestimates energy use during descent, which generally consists of energy-saving gliding to depth (Williams et al., 2000). By contrast, the ascent phase of a foraging dive typically requires steady swimming against negative buoyancy (Goldbogen et al., 2008; Goldbogen et al., 2006). Buoyancy will vary with body condition (i.e. fat stores) and the degree of lung collapse with depth, but here we assume that mean body density over the duration of the dive is essentially that of seawater. Because lung volume is relatively small in marine mammals (Snyder, 1983), particularly so in large baleen whales [measuring approximately 2.9% of body volume (Scholander, 1940; Smith and Pace, 1971)], the graded collapse of the lung with depth is not expected to increase energetic output above our active metabolic rate models (neutral buoyancy).

As a check, we calculated power output (using a combined efficiency of 0.15 to convert mechanical energy back to metabolic energy) during steady-state swimming at a mean speed determined from tag data. This cost was added to an estimate for maintenance costs generated from an allometric equation for basal metabolic rate (BMR) in large mammals (White et al., 2009). We also calculated the total cost of transport, including maintenance costs, using an allometric equation (Williams, 1999). Both power output estimates were 20–30% below values that we predict for AMR. For these reasons, we think that this is generally a conservative model, which errs on the side of overestimating locomotor costs. Thus, it is primarily intended to account for the costs of deeper and longer dives, where the cost is proportional to the time devoted to transit to and from the prey patches at depth rather than foraging.

Foraging effort: theoretical *vs* observed

Foraging effort was defined as the number of lunges executed per dive (lunge frequency). Lunge frequency was assumed to be an indicator of prey patch quality (Goldbogen et al., 2008), thus the highest lunge frequencies observed among tagged whales should represent maximum foraging effort. Because dive time is limited, only a certain number of lunges are theoretically possible. For these reasons, we predicted the maximum number of lunges that were possible at a given depth for a given dive time. Maximum dive duration was determined by the tag data. Specifically, we used the dive duration from only those dives that involved the highest lunge frequencies (one dive considered per individual). The time required for descent and ascent to a given depth was determined by mean body pitch angles and speed of the body. Bottom time, or the time available to execute lunges at the bottom of a dive, was equal to the difference between dive duration and the time spent ascending and descending to depth. We divided bottom time by the time required to perform the lunge (pre-engulfment acceleration, engulfment *per se*), and also by the time needed to filter the engulfed water mass, in order to calculate the theoretical lunge frequency maxima as a function of depth. Note that this approach does not incorporate predictions from optimal foraging theory, but instead only considers the maximum energy gain for a single dive.

Foraging efficiency

Energetic costs estimated for diving, filtering and surface recovery time were added to the energy expenditure required for lunge feeding. The energetic efficiency of foraging (Williams and Yeates, 2004) was defined as the ratio of the energy gained from ingested krill divided by all energy expenditures associated with the foraging dive including recovery time (see Appendix 2). The model accounted for the energy loss in assimilation of food and standard values for krill energy density (Lockyer, 1981; Lockyer, 2007). Because cetaceans exhibit elongated digestive tracks (Williams et al., 2001) that may be capable of microbial fermentation to enhance digestion efficiency (Herwig et al., 1984; Olsen et al., 2000), we assumed that are no physiological limits with respect to gastrointestinal capacity (Rosen et al., 2007). Furthermore, the extreme body size of blue whales suggests that they do not have to increase metabolic rate to maintain thermal balance (Lavigne et al., 1990; Ryg et al., 1993; Watts et al., 1993), even in polar waters, thus we assumed that there are no additional costs associated with life in cold water.

To assess the efficiency of a single lunge (i.e. at the sea surface where no diving costs are involved) we implemented our energetic

analysis independent of diving costs, but instead with respect to BMR predicted for large mammals (White et al., 2009). Accordingly, BMR was calculated using the allometric equation (Ahlborn, 2004):

$$\mathrm{BMR(W)} = 4M^{\mathrm{body}0.75}. \quad (4)$$

After accounting for energetic efficiency and all metabolic costs, a simple energy budget was used to estimate the number of lunges required for an average-sized blue whale to meet a daily energetic demand (*sensu* Goldbogen et al., 2007) as a function of prey density (see below). For example, prey biomass requirements for an average-sized blue whale (25 m) was taken as the mean from six different energetic models: 1120±359 kg krill individual^{-1} day^{-1} (Brodie, 1975; Croll et al., 2006). Foraging behavior (dive depth and duration) and lunge-feeding effort (number of lunges per dive) were determined by tag data averaged across all individuals in this study.

Prey density

For a given prey (krill) density and engulfment volume, we calculated the amount of prey obtained per lunge. We first considered krill density values measured by bongo net plankton tows (0.15 kg m^{-3}) at whale foraging locations at depth (Croll et al., 2005). This value probably represents a minimum estimate of krill density simply because krill can avoid nets using escape behavior (Hovenkamp, 1989). For example Croll et al. towed a 0.5 m^2 bongo net at a speed of approximately 1 m s^{-1} (Croll et al., 2005). By contrast, rorquals lunge at relatively higher speed (up to 5 m s^{-1}) with larger mouth apertures (>10 m^2), so we allowed krill density to increase within the model by over an order of magnitude higher than the values generated from net tows. Such a range in krill density is consistent with measurements using active acoustics (Cotte and Simard, 2005; Simard and Lavoie, 1999) and transparent nets (Brodie, 1978; Nicol, 1986), and this range is conservative with respect to the very high estimates from photographs (Dolphin, 1987; Hamner, 1984; Hamner et al., 1983; Nicol, 1986).

During the day, krill patches have been typically observed as dense and deep in order to avoid predation; at night, krill may disperse to facilitate feeding on phytoplankton located closer to the sea surface (Hewitt and Demer, 2000). Although this general trend may be biased because of acoustic methodology and the change in krill body orientation during the migration (Demer and Hewitt, 1995; Simard and Sourisseau, 2009), there is evidence that satiated krill begin to swim downward just after the initial upward migration towards the surface (Sourisseau et al., 2008), thereby decreasing overall density at the sea surface. Therefore, we explored two potential scenarios related to prey density: (1) krill density remains constant at all depths where lunges occurred, and (2) krill density decreases linearly with decreasing depth.

Results are presented as means ± s.d.

RESULTS

Kinematics of diving and lunge feeding

We successfully deployed tags on 265 blue whales and recorded data for at least one foraging dive for each individual (Table 1). We subsequently analyzed a total of 200 foraging dives, including 654 lunges at depth. Several whales exhibited continuous foraging effort, executing a rapid sequence of deep foraging dives (Fig. 1). Dive duration ranged from 3.1–15.2 min, but overall it was relatively consistent at 9.8±1.8 min. Similarly, maximum dive depth ranged widely from 52–315 m, but on average was 201±52 m. Surface recovery time between foraging dives varied from a single breath (16 s) to 6.7 min. However, across individuals, surface time was 2.7±1.1 min, during which a mean of 10±3 breaths were taken.

In general, the kinematics of diving in blue whales was similar to that of other rorqual whales. A characteristic foraging dive consisted of a gliding descent, multiple lunges at depth and an ascent powered by steady swimming. The proportion of time gliding during descent was 40±12%; however, in some cases either no gliding was evident at all or the whale was gliding for up to 95% of the descent. Blue whales generally adopted the same mean body angle during descent (–38±10 deg) and ascent (42±11 deg), although much steeper angles were sometimes observed (ranging from –65 to 66 deg), particularly during an ascent after a high number of lunges were executed. Whale speed during descent (2.6±0.5 m s^{-1}) was significantly higher than during ascent (1.6±0.5 m s^{-1}; P=<0.01, N=168), which we attributed to the negative buoyancy of the body associated with lung collapse under hydrostatic pressure.

The bottom phase of foraging dives averaged 5.7±1.5 min in duration (range: 1.3–11.7 min). Whales performed a mean of 3.5±1.1 lunges per dive (range: 1–6 lunges per dive). Kinematic data for a representative foraging dive are shown in Fig. 2. During a lunge, the speed of the body rapidly increased, powered by a bout of swimming strokes. The body angle at the moment of maximum velocity ranged from –12 to 80 deg, with a mean of 36±19 deg. During some foraging dives, there was a lunge at the very end of the descent phase that thus occurred at a significantly lower body angle. These lunges, on average, occurred when the body was horizontal (–5±7 deg), but in some instances they occurred at very steep (negative) body angles as low as –61 deg.

The number of lunges per dive (lunge frequency) was relatively constant at different depths (Fig. 3); there was no significant correlation between maximum dive depth and lunge frequency (P=0.299) or bottom time (P=0.254). Also, dive duration was not significantly correlated with dive depth (P=0.143). In theory, the number of lunges should have increased with decreasing depth because more time could be used foraging rather than traveling to and from the prey patch at depth (see dashed line in Fig. 3B). Furthermore, more dive time should theoretically be available at shallower depths because of the locomotor costs associated with diving deeper (see dashed line in Fig. 3A).

Maximum lunge speed was 3.7±0.4 m s^{-1} across all individuals. The full range in lunge speed, from 2.1 to 5.0 m s^{-1}, is depicted in Fig. 4. These speed profiles served as a guide for our hydrodynamic analyses and trajectory simulations during lunges. Each lunge record is illustrated by a light gray line and the average speed profile for each whale is shown by a blue line; the overall mean across all individuals is shown by the thick black line (Fig. 4). All simulations of engulfment, including variation in body size and drag coefficient, were superimposed on top of these speed profiles. In general, the model predictions provided a good match to the speed profiles generated from the tag data (Fig. 5).

Drag, work and power output during engulfment

We assessed the variance of drag, work and power output over a large range of blue whale body sizes, from 22 to 27 m in body length, with 20 lunge-feeding simulations (Appendix 1). Our hydrodynamic analyses suggest that total peak drag during engulfment ranged from 58±11 kN to 116±26 kN for the smallest and largest blue whales considered, respectively. Mass-specific values for total peak drag were generally independent of body size at approximately 1 N kg^{-1}. Total work against drag during engulfment *per se* ranged from 290±40 to 730±160 kJ, whereas mass-specific values ranged from 4.8±0.7 to 6.0±1.3 J kg^{-1}. Power output during engulfment varied

Table 1. Kinematic data for blue whale foraging dives

Date (m/dd/yyyy)	Location	No. of foraging dives	Dive duration (min)	Dive depth (m)	No. of lunges per dive	Surface time (min)	Descent time (min)	Descent angle (deg)	Descent speed (m s^{-1})	Gliding phase of descent (%)	Ascent time (min)	Ascent angle (deg)	Ascent speed (m s^{-1})	Lunge angle, type A (deg)	Lunge angle, type B (deg)
6/30/2002	LJ	24	10.1	154	1.6	1.0	2.3	n/a	n/a	n/a	2.7	n/a	n/a	–	n/a
7/24/2003	SNI	5	11.0	261	2.8	3.5	2.3	–58	n/a	26	3.4	56	n/a	–6	67
7/24/2003	SNI	3	10.7	261	3.7	3.7	2.0	n/a	n/a	n/a	2.8	n/a	n/a	–	n/a
8/22/2003	TCB	1	12.1	259	5.0	4.0	2.2	–37	2.7	22	2.4	49	1.7	–5	5
8/22/2003	TCB	1	11.3	266	5.0	3.8	1.9	–51	2.4	23	2.5	57	1.5	–	18
9/24/2003	MB	4	11.7	226	5.5	3.8	1.8	–42	2.9	25	2.1	58	1.5	–6	31
9/26/2003	MB	12	10.1	226	3.1	3.1	2.0	–39	2.9	25	2.4	44	1.6	–	64
9/28/2003	MB	4	9.4	269	3.8	4.5	1.7	–51	3.0	26	2.1	50	1.7	–	61
7/20/2004	MB	7	9.2	290	3.1	2.8	2.0	–38	3.2	29	2.9	51	1.5	–13	34
7/21/2004	SBC	3	7.9	146	3.0	1.4	1.9	–30	2.0	32	1.7	45	1.6	–6	19
3/04/2004	SBC	3	11.8	125	5.3	2.1	1.5	–24	2.0	36	1.1	37	0.8	–	42
3/04/2004	SC	7	7.9	161	1.9	1.5	2.2	–27	3.0	38	1.8	30	2.3	–	60
8/09/2005	SC	6	5.7	70	2.3	1.5	1.3	–24	2.7	39	0.8	22	2.7	–	51
8/10/2005	MB	1	12.8	196	4.0	5.2	1.5	–36	2.7	39	2.4	24	1.6	–	43
8/10/2005	MB	1	10.2	155	3.0	4.2	1.4	–20	3.7	42	2.3	27	2.5	–	13
9/09/2005	MB	4	10.1	192	1.5	1.6	2.9	–21	3.0	44	2.3	29	2.4	0	22
9/12/2005	MB	3	11.1	200	2.3	1.8	2.3	–33	1.8	48	2.1	39	1.4	4	41
9/06/2007	MB	13	11.5	157	4.3	2.6	2.3	–32	1.6	48	2.2	33	1.2	8	14
9/06/2007	SBC	2	10.1	221	3.0	1.9	1.7	–50	2.5	55	3.1	35	1.3	–	51
9/06/2007	SBC	22	8.7	198	2.8	1.6	1.4	–45	2.9	57	2.6	45	1.2	–10	26
9/07/2007	SBC	17	9.3	217	3.2	3.4	2.1	–35	2.3	57	2.2	41	2.0	–7	7
9/07/2007	SBC	2	10.1	210	4.5	2.8	2.3	–43	2.1	52	2.4	48	1.6	–6	17
9/08/2007	SBC	13	5.9	152	3.8	1.4	1.0	–37	3.3	53	1.2	54	1.6	–17	31
9/08/2007	SBC	31	8.2	175	4.0	2.5	1.7	–42	2.5	49	2.1	39	1.3	–2	32
9/08/2007	SBC	11	8.5	225	3.9	3.0	1.6	–53	2.4	52	2.1	56	1.5	2	59
Mean of means			9.8	201	3.5	2.7	1.9	–38	2.6	40	2.2	42	1.6	–5	36
Standard deviation of means			1.8	52	1.1	1.1	0.4	10	0.5	12	0.6	11	0.5	7	19
Minimum of all dives			3.1	55	1	0.2	0.4	–65	1.2	0	0.4	10	0.7	–61	–12
Maximum of all dives			15.2	315	6	6.7	6.8	–8	4.0	95	5	66	2.8	12	80

LJ, La Jolla, CA; MB, Monterey Bay; SBC, Santa Barbara Channel; SC, Sea of Cortez; SNI, San Nicholas Island; TCB, Tanner-Cortez Banks.
–, did not occur; n/a, not applicable. Type A lunges occurred at the end of descent; Type B lunges occurred at the bottom of the dive.

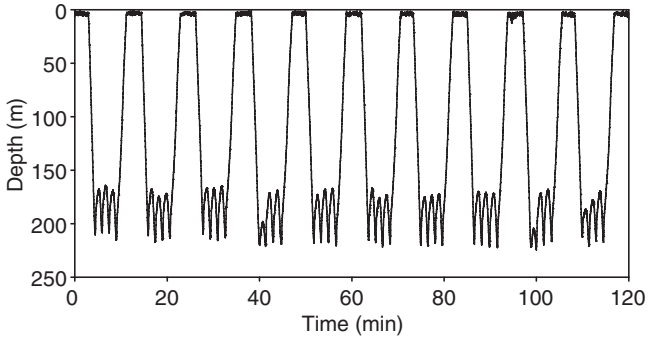

Fig. 1. Continuous deep foraging dives. A mean of four lunges were executed per dive. Note the approximately 50 m vertical excursion associated with each lunge at depth.

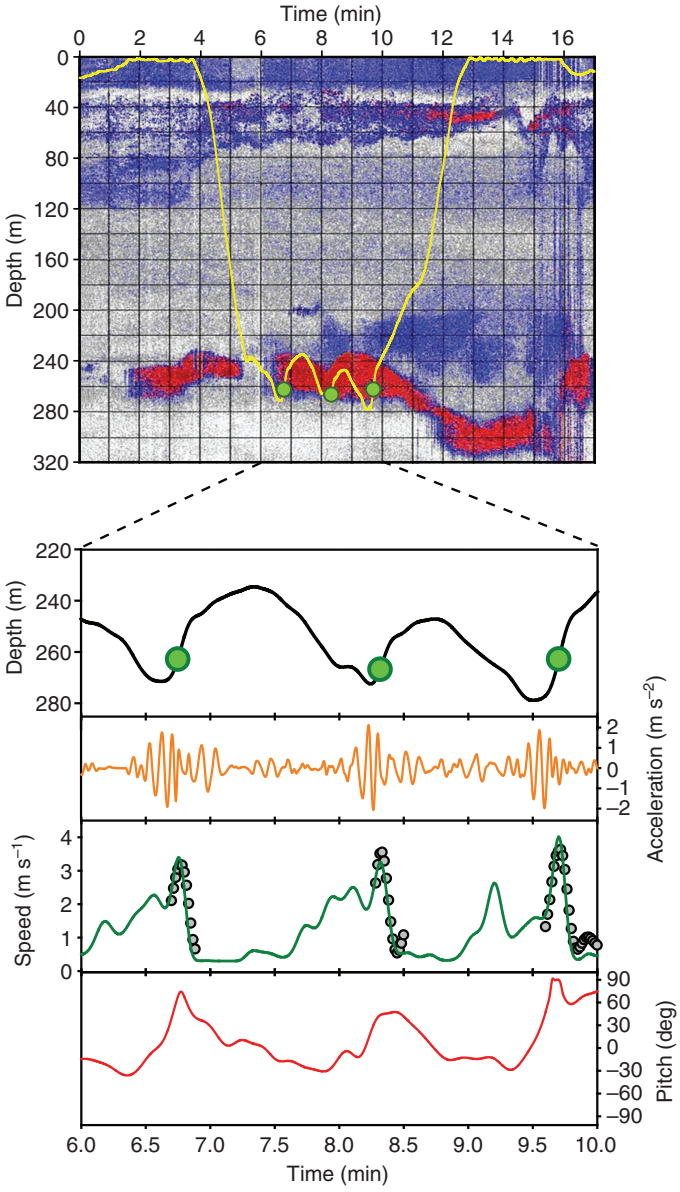

Fig. 2. Kinematics of a blue whale foraging dive. The upper panel shows the dive profile (yellow line), with lunges highlighted (green circles), superimposed on a prey field map showing qualitative changes in krill density (white, low; blue, medium; red, high). The lower panels show the detailed kinematics during lunges at depth. Here, the dive profile is shown by a black line. The orange line shows fluking strokes derived from the accelerometer data, the green line represents speed estimated from flow noise, and the grey circles indicate the speed calculated from the vertical velocity of the body divided by the sine of the body pitch angle, which is shown by the red line.

from 47±11 to 101±32 kW, and mass-specific values were approximately 0.83±0.25 W kg^{-1}. Note that these values for work and power are purely mechanical costs, and do not account for the efficiency (using a combined efficiency of 0.15) of converting mechanical energy into metabolic energy. Thus, the total metabolic energy and power expended as a result of drag ranged from 31.7±4.7 to 39.7±8.8 J kg^{-1} and 5.2±1.2 to 5.5±1.8 W kg^{-1}, respectively.

An example of a lunge-feeding simulation for a 25 m blue whale is shown in Fig. 5. We only used simulations for bioenergetic analyses that could reproduce the trajectory of the whale's body during the lunge (dashed line), as determined by digital tag data (circles with error bars that correspond to ±1 s.d.; Fig. 5A). The simulation tracked the expansion of the buccal cavity and, therefore, the magnitude of the engulfed water mass [posterior to the temporomandibular joint (TMJ)] was known at any point in time (gray line). Each lunge consisted of a typical two-phase engulfment sequence (Fig. 5B): mouth opening, followed by mouth closure, both of which were equal in duration (Goldbogen et al., 2007). The mouth opening phase ($0<t<3.3$ s, where t is time) was coupled to the forward push of engulfed water, whereby the musculature within the VGB system undergoes eccentric contraction to resist inflation of the buccal cavity (Potvin et al., 2009). This push generates a novel source of drag (engulfment drag) that increases in concert with both the speed and magnitude of the engulfed water mass (Fig. 5C). The active shove of engulfed water was nonexistent during mouth closure ($3.3<t<6.6$ s) and, therefore, was dominated solely by shape drag, which represents the drag generated from flow around the body (this issue is further discussed in Appendix 1).

Energetic efficiency

After accounting for the efficiency of converting metabolic energy into mechanical energy, the total energetic cost of a single lunge, including pre-engulfment acceleration, ranged from 3226 to 8071 kJ (Table 2). Energy loss attributed to both BMR expenditure during the lunge (~20 s) and the time required to filter the engulfed mass (~55 s) varied from 1169 to 1966 kJ, as determined by Eqn 4. In general, the cost of a lunge was approximately four times BMR (for the duration of the lunging and filtering phases). Costs of both lunging and filtering were dwarfed by the energy gained from captured krill, ranging from 34,776 kJ at the lowest prey density considered (0.15 kg m^{-3}) to 1,912,680 kJ at the highest density (4.5 kg m^{-3}). Thus, the energetic efficiency of a single lunge ranged from 6.5 to 237, depending on the density of krill.

After accounting for diving costs, the energetic efficiency of a typical deep foraging dive, which involved a mean of 3.5 lunges per dive (Table 3), was substantially lower compared with that of a single lunge (Table 2). At any prey density considered, the efficiency of the dive was approximately 2.5 times lower than that of a single lunge. This effect was attributed to the increased cost of transit relative to the energy gained from multiple lunges at depth. Foraging efficiency increased with krill density and was generally still high, up to 90, at the highest observed krill density considered in the model.

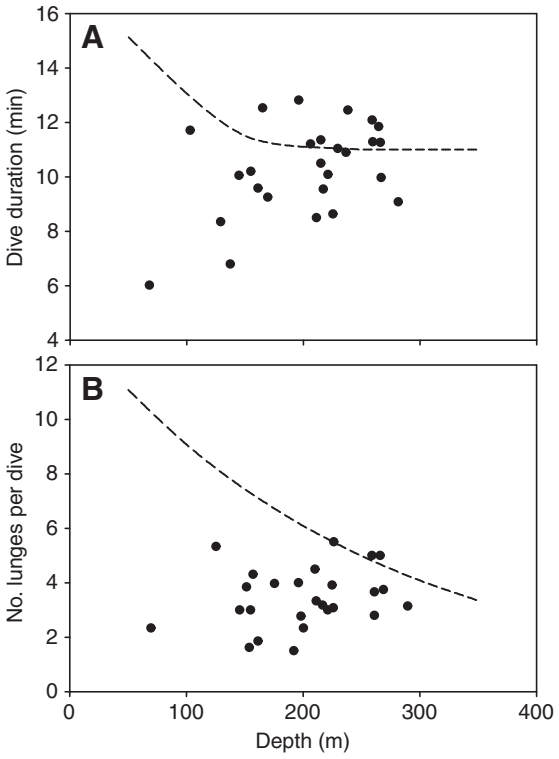

Fig. 3. Dive duration (A) and lunge feeding effort (B) as a function of maximum dive depth. Mean values for each tagged whale are shown by filled circles. Mean dive duration (across individuals) for deep dives (>150 m) was 11 min. This value was chosen for modeling the energetics of deep dives (dashed line in A). Shallower dives were assigned progressively longer durations up to 15 min, which was the longest recorded (Table 1). With more dive time available, more lunges should theoretically be possible (dashed line in B). There was no significant correlation between dive depth and dive duration or the number of lunges per dive.

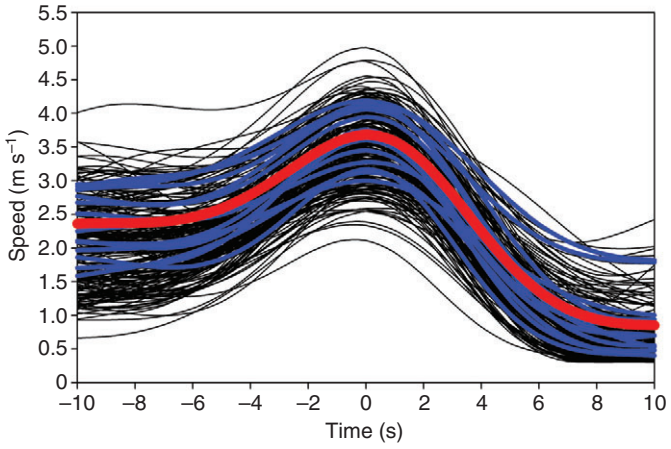

Fig. 4. Speed profiles during lunges. Each lunge is shown by a black line and the average speed profile for each individual is shown by the blue lines. The overall mean across all individuals is shown by the thick red line.

If prey density remained constant within the model, we predicted that foraging efficiency should increase with decreasing depth because, in theory, more lunges should be possible at shallower depths (Fig. 6A). However, when the model was parameterized with tag data, efficiency was relatively constant because shallower dives still exhibited the same number of lunges as deeper dives (Fig. 3). By contrast, if prey density was allowed to increase with depth, theory predicted a steady decrease in efficiency when foraging at shallower krill patches (Fig. 6B). The same pattern was found when the model was parameterized with tag data, owing to the strong dependence of feeding efficiency on prey patch density. Under both prey density scenarios, the model output with tag data was always lower than theoretical model results. This result probably occurred because theory did not account for time spent searching for prey patches during the bottom phase of the dive.

We extrapolated our analysis for longer time scales to determine how many lunges were needed, as a function of krill density, to meet a daily energetic demand (Fig. 7). The model response shows an exponential decrease in foraging effort with increasing krill density. For a typical deep foraging dive of 9.8 min, including a mean of 2.7 min in surface time, the amount of foraging time required to execute the predicted number of lunges was also determined. For example, we predicted that approximately 40 lunges, or 2.5 h of foraging time, was required at a krill density of 0.5 kg m^{-3}. Our analysis also predicted a critical density, 0.1 kg m^{-3} (dashed line in Fig. 7), below which a blue whale will be unable to meet energetic demands even during continuous deep-diving foraging effort.

DISCUSSION

Foraging costs and energetic efficiency

The efficiency at which animals obtain and use energy has a significant impact on reproductive fitness, life history and ecosystem function (Boyd, 2002). A general characteristic of baleen whale life history is the annual migration between feeding areas in highly productive areas at high latitudes and breeding grounds at lower latitudes (Clapham, 2001; Corkeron and Connor, 1999; Rasmussen et al., 2007). The extended periods of time spent in oligotrophic waters with limited prey suggest that migrating cetaceans must rely heavily on the energy stored within the blubber layer (Brodie, 1975). This lipid cache is built up during intensive feeding bouts in the summer months (see Fig. 1) and has been demonstrably correlated with increases in food availability and reproductive success (Lockyer, 1986). Because energy use and gain occurs at such large temporal and spatial scales, baleen whales are predicted to have efficient feeding mechanisms that maximize net energy gain (Goldbogen et al., 2010; Goldbogen et al., 2007).

Our analysis suggests that the efficiency of a single lunge in blue whales (i.e. at the sea surface, thus no diving costs were considered), defined as the ratio of energy acquired from ingested prey to energy expended during lunge feeding, can have very high values if prey density is also high. A single blue whale lunge had an efficiency of approximately 7 at low krill densities and over 200 at higher densities (Table 2). We attribute this differential efficiency to the high energy gain from ingested krill relative to the relatively low energy expenditures from drag and BMR. Our calculations demonstrate that the energy required to overcome drag and accelerate the engulfed water mass was approximately twice that of maintenance costs predicted from BMR during the time period of the lunge (including the filtering phase). Although this finding supports the general hypothesis of high feeding costs in rorquals, this difference in blue whales was not as high as expected considering the high drag that is associated with the lunge-feeding mechanism (Potvin et al., 2009).

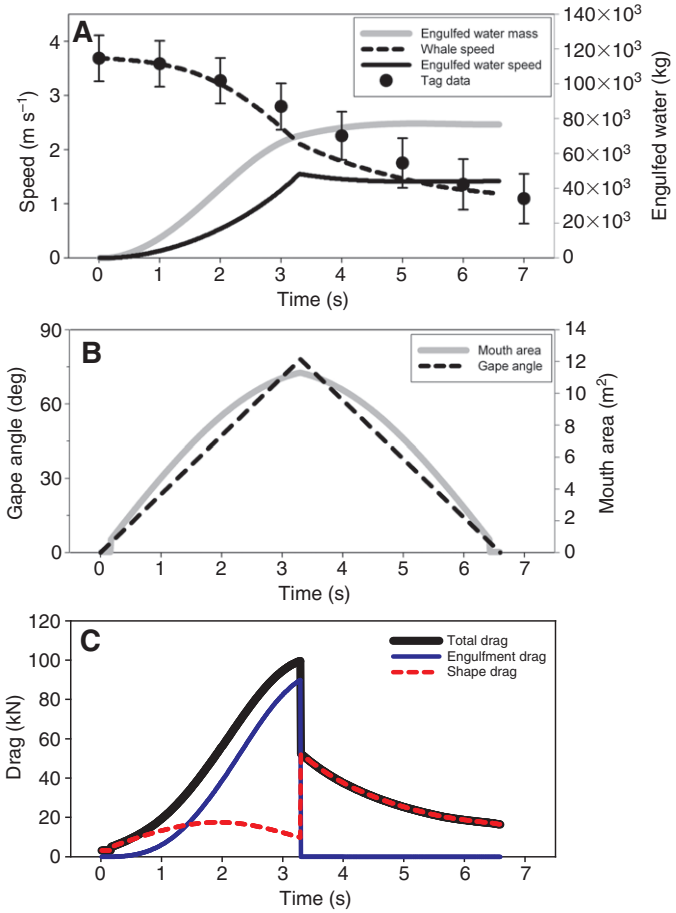

Fig. 5. Mechanics and hydrodynamics of a blue whale lunge (25 m body length). (A) Each simulation predicted the trajectory of whale (dashed line) and engulfed water (solid black line). The model also calculated the instantaneous magnitude of the engulfed water mass (grey line). Tag data are means ± 1 s.d. (B) Gape angle dynamics (dashed line) predicted by the model (t_{engulf}=6.6 s) was corroborated by video data of blue whale lunges (t_{engulf}=7.3±0.7 s). (C) Two components of drag during active engulfment vary as a function of time. The mouth-opening phase (0–3.3 s) is dominated by engulfment drag (internal), caused by the acceleration of engulfed water. By contrast, the mouth-closing phase (3.3–6.6 s) consists only of shape drag (due to flow around the body).

During a lunge, drag reaches extremely high values, up to several times the drag experienced during steady-state swimming. However, metabolic rate may have been overestimated because: (1) BMR was extrapolated from values obtained from smaller mammals (White et al., 2009), and (2) approximately 27% of blue whale body mass consists of blubber (Lockyer, 1976), which has a much lower metabolic rate than other tissue types (Brodie, 1975). Even if our estimates of BMR are accurate, the drag during a lunge is sustained for only several seconds (Fig. 5C), thereby minimizing energy loss despite the mouth being agape at high speed. Furthermore, most of the body's kinetic energy that is used to power the lunge is built up during the pre-engulfment acceleration phase (Figs 2 and 4), which should involve much lower drag and thus lower energy expenditure.

After the costs of diving were taken into account, the overall energetic efficiency of blue whale lunge feeding was lower, ranging from approximately 3 to 90 (Table 3). However, at the highest observed prey densities (4.5 kg m^{-3}), the efficiency of blue whale foraging dives (90±2) was nearly an order of magnitude higher than other marine mammals. These values ranged from 3.8 in sea otters (*Enhydra lutra*) to 10.2 in Weddell seals (*Leptonychotes weddellii*) (Williams and Yeates, 2004). The driving factor behind the high efficiency of blue whale lunge feeding was krill density (Tables 2 and 3; Fig. 6B). It is possible that lunge-feeding efficiency could be even higher if denser patches of krill can be exploited. Some estimates of krill density from photographs generate extremely high values of 30,000 individuals m^{-3} for *Euphausia superba* (Hamner, 1984; Hamner et al., 1983), 50,000 individuals m^{-3} for *Thysanoessa raschii* (Dolphin, 1987) and 770,000 individuals m^{-3} for *Meganyctiphanes norvegica* (Nicol, 1986). These density estimates exceed the highest value considered in this study by several orders of magnitude, and thus we suspect that foraging efficiency could reach values exceeding 1000 if these types of patches can be successfully located and engulfed.

The cost of lunge feeding *per se* accounted for 38–57% of the total cost of a foraging dive (Table 3), which was higher than the estimate (10–36%) found for sustained foraging sprints during deep dives in short-finned pilot whales (*Globicephala macrorhynchus*) (Soto et al., 2008). The cost of blue whale lunge feeding compared with the cost of diving was still lower than expected, considering the brevity of their foraging dives with respect to their body size. Previous researchers calculated a theoretical aerobic dive limit (TADL) of 31.2 min for blue whales (Croll et al., 2001), but foraging dive durations are consistently less than half the predicted TADL (Table 1). Thus, we expected *a priori* that blue whale lunge-feeding costs would be at least equal to the cost of diving. One explanation is that we may have overestimated the cost of diving using AMR, which was 2 to 3 times above basal metabolic rate. Note that AMR was applied to the entire duration of the dive, including time spent gliding during descent and the filter phase between lunges at depth, during which swimming activity was kept to a minimum. Gliding is a hallmark of the energy-conserving behavioral repertoire for diving marine mammals (Williams et al., 2000). This locomotor strategy, coupled with a low cost of transport (Williams, 1999) and diving bradycardia (Williams et al., 1999), suggests that our use of AMR may overestimate diving costs for the majority of the dive (Fahlman et al., 2008a). Thus, by underestimating prey density and overestimating diving costs, our calculations of foraging efficiency may represent conservative (i.e. minimum) values.

Unlike rorquals, foraging costs in some marine mammals can be measured directly from oxygen consumption during post-dive recovery periods at the sea surface. This technique, combined with video-data logging, has shown that the cost of foraging increases linearly with the number of strokes performed during the dive in Weddell seals (Williams et al., 2004). As with running terrestrial animals, this mass-specific cost per stroke was invariant with body size in phocid seals (Williams et al., 2004). Theoretically, not all strokes can be considered equal (i.e. strokes used for steady swimming versus acceleration) and, in rorquals, some of these strokes occur when the body is being accelerated up to lunging speed or during the deceleration phase of the lunge when the whale performs work to overcome high drag and to accelerate the engulfed water mass (Fig. 2). If blue whales require approximately 6 strokes to execute a lunge (Fig. 2), the cost of a lunge is estimated at 10.2±1.2 J kg^{-1} stroke^{-1}. Although this value represents a higher relative cost than for both terrestrial mammals (5.0 J kg^{-1} stroke^{-1}) and phocid seals (1.44–2.87 J kg^{-1} stroke^{-1}), it is well within an order of magnitude. Thus, despite the very high drag associated with lunge feeding, the energetic cost per stroke is not that great relative to body size. We attribute such a low mass-specific cost per stroke to

Table 2. Effects of prey density on the energetic efficiency of a single blue whale lunge

Krill density (kg m^{-3})	Body length (m)	Body mass (kg)	Engulfment volume (m^3)	Krill obtained (kg)	Gross energy gain (kJ)	Energy loss, lunge (kJ)	Energy loss, BMR (kJ)	Energy loss, total (kJ)	Net energy gain (kJ)	Efficiency, lunge
0.15	22	61,318	60	9	34,776	3226	1169	4395	30,381	7.9
	25	96,568	80	12	46,368	6301	1643	7944	38,424	5.8
	27	122,605	110	17	65,688	8071	1966	10,037	55,651	6.5
0.50	22	61,318	60	30	115,920	3226	1169	4395	111,525	26
	25	96,568	80	40	154,560	6301	1643	7944	146,616	19
	27	122,605	110	55	212,520	8071	1966	10,037	202,483	21
1.65	22	61,318	60	99	382,536	3226	1169	4395	378,141	87
	25	96,568	80	132	510,048	6301	1643	7944	502,104	64
	27	122,605	110	182	703,248	8071	1966	10,037	693,211	70
4.50	22	61,318	60	270	1,043,280	3226	1169	4395	1,038,885	237
	25	96,568	80	360	1,391,040	6301	1643	7944	1,383,096	175
	27	122,605	110	495	1,912,680	8071	1966	10,037	1,902,643	191

BMR, basal metabolic rate. Gross energy gain is the krill mass × energy density (4600 kJ kg^{-1}) × assimilation efficiency of 0.84. Energy loss BMR is obtained from Eqn 4 and average lunge time of 75 s. Efficiency is the ratio of gross energy gain to the total energy loss in one lunge.

the acute positive allometry of body mass (M_{body}) exhibited by blue whales ($M_{body} \propto L_{body}^{3.5}$, where L_{body} is body length; r^2=0.89, P<0.05, N=48).

An underappreciated 'cost' associated with lunge feeding is the time that must be devoted to filtering the engulfed water mass, which constitutes approximately one-third of a typical foraging dive. Filter time is determined by the magnitude of the engulfed water volume, the speed at which water is filtered past the baleen and the effective area of the baleen. Assuming that baleen functions as a cross-flow filter that processes water at speeds less than 1 m s^{-1} (Goldbogen et al., 2007), the prime determinant of filter time is the ratio of engulfed water volume to baleen area. The magnitude of the engulfed water mass (M_w) increases allometrically ($M_w \propto L_{body}^{3.5}$) because of the positively allometry of the engulfment apparatus (skull, mandibles and buccal cavity) relative to the rest of the body (Goldbogen et al., 2010). Baleen area is expected to be proportional to mouth area (A_{mouth}), which also scales allometrically ($A_{mouth} \propto L_{body}^{2.4}$), but not as steeply as engulfment capacity. Therefore, larger rorquals must filter relatively more engulfed water with proportionally less baleen area, which yields longer filter times in between consecutive lunges at depth. Accordingly, the mean filter time for blue whales in this study was 55±10 s, which is significantly higher than values for fin whales (Goldbogen et al., 2006) and humpback whales (*Megaptera novaeangliae*) (Goldbogen et al., 2008). However, it is still possible that rorquals of different sizes achieve the same overall volumetric filter rate if the putative fractal design of the baleen filter (i.e. its effective filtering area) exhibits positive allometry relative to the size of the skull (Alexander, 1998).

Theoretical *versus* observed foraging behavior

We hypothesized that the number of lunges per dive (lunge frequency) should increase with decreasing dive depth if blue whales were to maximize prey capture for a single dive. Theoretically, more time can be devoted to lunge feeding at shallower depths because: (1) less time is spent in transit to and from the prey patch, and (2) diving costs should be lower. However, we found that lunge frequency was the same regardless of dive depth (Fig. 3B). It is thought that lunge frequency may be an indication of prey patch quality (i.e. prey density) because lunge frequency was positively correlated with ascent and descent body angles (Goldbogen et al., 2008). To fully exploit high-quality prey patches, rorquals should exhibit high lunge frequencies at depth and return to the surface at steep body angles to minimize transit time. When poor prey patches are encountered at depth, the dive will be terminated, resulting in lower lunge frequencies that are then followed by shallow body angles on ascent. By adopting shallow dive angles, animals can

Table 3. Effects of prey density on the efficiency of blue whale foraging dives

Krill density (kg m^{-3})	Body length (m)	Body mass (kg)	Volume filtered, total (m^3)	Krill obtained (kg)	Gross energy gain (kJ)	Energy loss, lunge (kJ)	Energy loss, diving (kJ)	Energy loss, total (kJ)	Net energy gain (kJ)	Efficiency, dive
0.15	22	61,318	210	32	123,648	11,292	29,475	82,881	82,881	3.0
	25	96,568	280	43	166,152	22,053	41,403	102,696	102,696	2.6
	27	122,605	385	58	224,112	28,250	49,499	146,363	146,363	2.9
0.50	22	61,318	210	105	405,720	11,292	29,475	364,953	364,953	10
	25	96,568	280	140	540,960	22,053	41,403	477,504	477,504	8.5
	27	122,605	385	193	745,752	28,250	49,499	668,003	668,003	9.6
1.65	22	61,318	210	347	1,340,808	11,292	29,475	1,300,041	1,300,041	33
	25	96,568	280	462	1,785,168	22,053	41,403	1,721,712	1,721,712	28
	27	122,605	385	635	2,453,640	28,250	49,499	2,375,891	2,375,891	32
4.50	22	61,318	210	945	3,651,480	11,292	29,475	3,610,713	3,610,713	90
	*25	96,568	280	1,260	4,868,640	22,053	41,403	82,881	4,805,184	77
	27	122,605	385	1,733	6,696,312	28,250	49,499	102,696	6,618,563	86

All calculations correspond to foraging dives that average 200 m deep and a lunge frequency of 3.5 lunges per dive; dive duration was 9.8 min followed by a surface recovery period of 2.7 min, as determined from tag data (Table 1). Gross energy gain represents the energy density of krill after accounting for assimilation efficiency. The energetic cost of diving represents all costs that are not associated with lunge feeding *per se*, except for the filter phase between lunges. Efficiency is the ratio of gross energy gain to the total energy loss in a dive. *Data in this row used in Fig. A1.

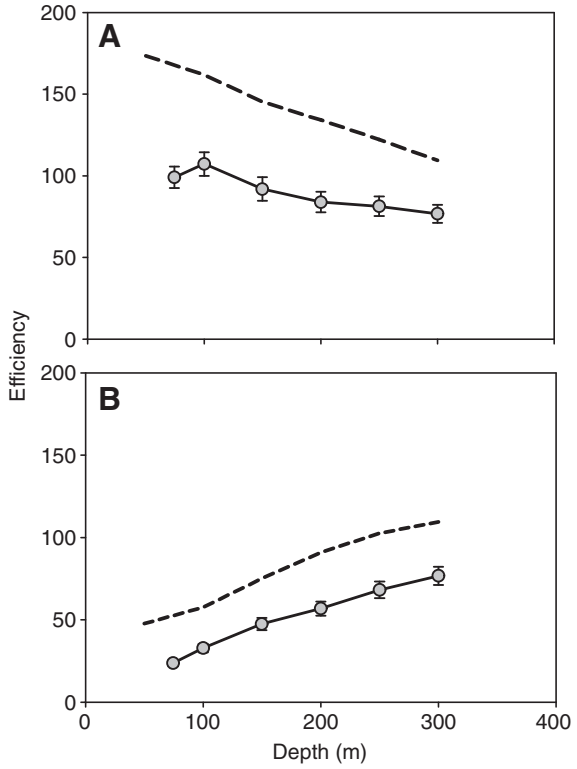

Fig. 6. Energetic efficiency of foraging dives. (A) When krill density was assumed to be constant with depth, the energetic efficiency should have theoretically increased with decreasing depth (dashed line) because more lunges are possible at shallower depths for a given amount of dive time. However, tag data demonstrated that lunge frequency was invariant of dive depth (Fig. 3) and, therefore, efficiency was also irrespective of depth (solid line) and the costs associated with diving. (B) When krill density decreased linearly with decreasing depth (from 4.5 kg m^{-3} at 300 m to 0.1 kg m^{-3} at 75 m), foraging efficiency also decreased. Data are means ± 1 s.d. for the range in blue whale body length from 22 to 27 m.

maximize the horizontal area covered and increase the chance of locating a higher quality prey patch (Sato et al., 2004).

For these reasons, we attributed the lunge frequency patterns we observed (Fig. 3B) to a general decrease in prey density with decreasing depth. One alternative explanation is that prey patches are further apart in space, which would result in more transit time between consecutive lunges at depth, thereby allowing less time available for lunges. However, we also found that dive duration was not correlated with dive depth (Fig. 3A). This finding suggests that blue whales did indeed terminate dives before oxygen stores were fully exhausted because, in theory, shallower dives could be longer in duration. Furthermore, we found a positive correlation between mean lunge frequency and mean ascent body angle across individuals (r=0.537, P=0.00695, N=173), which supports the hypothesis that the number of lunges per dive is an indication of prey patch quality. Blue whales may also choose not to perform long dives at shallower depths because they could instead return to the surface to breath during the filter phase after each lunge (Ware et al., 2010). Such a strategy effectively decreases post-dive surface time, by only needing to breathe once or twice in between each lunge, and thus facilitates relatively continuous foraging near the sea surface. Under this scenario, the number of lunges per dive will progressively decrease with decreasing depth (Ware et al., 2010), which is contrary to the prediction presented here on the basis of maximizing prey capture for just a single deep foraging dive.

If krill density decreased with decreasing depth, it may be related to the diel vertical migration of krill. A general observation is that daytime krill patches at depth are dense, but at night they migrate toward the sea surface and disperse to feed (Hewitt and Demer, 2000). Researchers have been unable to definitively assess density changes of krill patches during the vertical migration because of the differential day–night bias of both acoustic and net tow sampling techniques (Simard and Sourisseau, 2009). Nevertheless, there is evidence that krill return to depth once they are satiated (Sourisseau et al., 2008), which should decrease the overall nighttime density at the sea surface. A recent study has shown, however, that when dense krill patches are sustained at the sea surface, humpback whales will continue to feed into the night (Ware et al., 2010).

All of our deployments that remained attached into the night showed a concomitant decrease in dive depth and lunge frequency near dusk, followed by a behavioral switch to resting behavior at the sea surface (<50 m depth). These results are supported by previous tag studies that also show this marked transition in foraging behavior associated with dusk in both blue whales (Calambokidis et al., 2007; Croll et al., 1998; Fiedler et al., 1998; Oleson et al., 2007) and fin whales (Panigada et al., 2003). Simultaneous tracking of tagged blue whales and krill aggregations at depth demonstrate that blue whales follow their diel migration and continue feeding until the scattering layer reaches the sea surface at night [see fig. 6 in Fiedler et al. (Fiedler et al., 1998) or fig. 5 in Croll et al. (Croll et al., 1998), and fig. 3 in Calambokidis et al. (Calambokidis et al., 2007)]. We hypothesize that this halt in

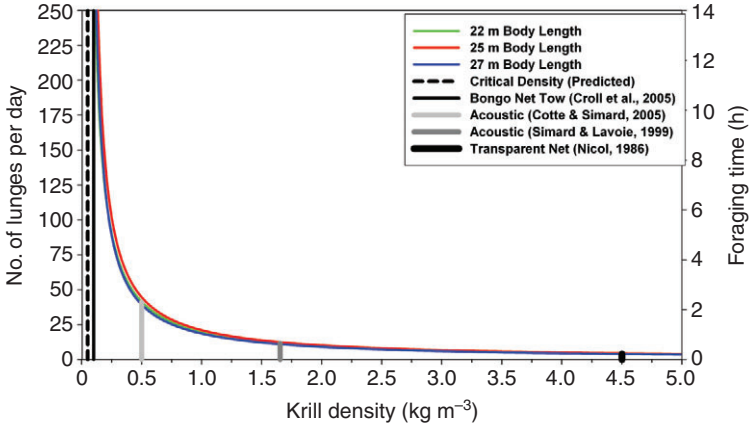

Fig. 7. Effects of krill density on the energetic efficiency of foraging. After accounting for the costs of diving and lunge feeding (Tables 2, 3), the model predicted the number of lunges required to meet standard energetic demands for a 24 h period (left axis). Assuming continuous feeding to an average depth and duration (followed by surface recovery time), as determined by tag data (Table 1), we calculated the amount of foraging time that is required to meet this daily energetic requirement of approximately 1000 kg of krill. These estimates are represented by the curved, colored lines for blue whales of three different sizes (22, 25 and 27 m). The solid vertical lines indicate krill density estimates using different techniques that correspond to the reference values used for the bioenergetic analyses summarized in Tables 2 and 3. The vertical dashed line represents the critical density (0.1 kg m^{-3}) at which a blue whale will start to loss body mass, even if foraging is continuous over the course of the 24 h period.

foraging behavior at night is related to a foraging threshold that is related to a critical density in prey (Fig. 7). Below this critical density, the efficiency of lunge feeding is significantly decreased and a net loss of energy is predicted, even if the whale forages continuously.

An alternative explanation for this diel foraging pattern is that blue whales cannot feed at night because they fail to visually locate krill without downwelling sunlight. However, there is limited evidence that humpback whales feed at night using putative echolocation (Stimpert et al., 2007) or tactile mechanisms (Friedlaender et al., 2009). Crittercam deployments on blue whales show that daytime foraging dives often involve lunges at steep upward pitch angles [see fig. 4 in Calambokidis et al. (Calambokidis et al., 2007); cf. Fig. 2], where krill patches are backlit from downwelling sunlight (Calambokidis et al., 2007). However, these authors also reported lunges that occurred at the end of the initial descent [see fig. 5 in Calambokidis et al. (Calambokidis et al., 2007)], which is similar to what we report here for 14 of 26 tagged blue whales (lunge type A, Table 1). The decision to lunge on descent *versus* ascent (during the bottom phase of a dive) may be related to the location of the prey patch upon initial descent. We envision a scenario in which a diving whale that descends directly into the prey field would initiate a lunge upon the detection of a sufficient number of prey hits against sensory tubercles or vibrissae located on the snout (Ogawa and Shida, 1950; Slijper, 1979). If a prey patch is detected visually before it is detected mechanically, the whale would have to maneuver and lunge into the prey field on ascent (Fig. 2). We suggest, therefore, that rorquals employ a variety of sensory modalities to locate and capture prey. Future research that combines three-dimensional analyses of both the prey field and lunge-feeding whales are required for a better understanding of how rorquals exploit prey patches at depth.

APPENDIX 1. BASIC LUNGE-FEEDING MODEL (BLFM) – A SUMMARY

The BLFM – version 2.0

The energetics of the engulfment phase are calculated by modeling the interaction between a whale's body and the mass it engulfs and its resulting impact on the motions of both bodies. We describe here an upgraded version of the BLFM originally proposed by Potvin et al. (Potvin et al., 2009), in which the engulfment time scale and gape opening rates are now calculated functions rather than empirical inputs (Potvin et al., 2010). Note that this current version does not include the modeling of the pre-engulfment and purging stages, even though they are part of a lunge.

The BLFM simulates the trajectories of both whale and (growing) engulfed mass as a head-on collision that occurs along a straight-line trajectory. Such a trajectory may be horizontal or angled depending on the specifics of a lunge. The Newtonian equations of motion for each body are given by:

$$M_c a_c(t) = T(t) - F_{ED}(t) - F_{SD}(t) + F_{ext}, \quad \text{(A1)}$$

$$M_w(t)a_w(t) + \psi V_w(t)\rho_w A_c(t)[V_c(t) - V_w(t)] = F_{BC}(t) - F_{ww}(t), \quad \text{(A2)}$$

where ρ_w is the density of seawater (1025 kg m^{-3}); M_c and a_c, and $M_w(t)$ and a_w correspond to the mass and acceleration of an empty whale (cetacean) and engulfed water, respectively. These accelerations are defined from $a_c = dV_c/dt$ and $a_w = dV_w/dt$, with the velocities $V_c(t)$ and $V_w(t)$ measured from a fixed reference frame. The forces applied on the whale and engulfed mass appear on the right-hand side of these equations. As previously illustrated [see fig. 2 in Potvin et al. (Potvin et al., 2009)], these forces include: (1) the muscle action (F_{BC}) applied along the buccal cavity wall against the engulfed mass, which by reaction gives rise to the engulfment drag (F_{ED}) component of the total drag sustained by the whale; (2) the fluking thrust (T), visualized here as pointing forward and parallel to the motion, whether horizontal or angled; (3) the external force (F_{ext}), consisting of the whale's weight, minus buoyancy, as projected along the axis of motion; (4) the so-called shape drag force (F_{SD}) corresponding to the flow moving around the body; and (5) the water-to-water drag force (F_{ww}), i.e. the 'push' of 'the rest of the ocean' against the exposed end of the engulfed water (mouth side). The specific values and functions used for these forces are described in the next section. Note that Eqn A1 does not include the effects of the lift generated by the body, fluke and flippers, as recently discussed (Cooper et al., 2008).

The function $M_w(t)$ tracks the water accumulating in the buccal cavity as calculated *via* an integration over the flux of fluid entering the cavity:

$$M_w(t) = \psi\rho_w \int_0^t dt' A_c(t')\left[V_c(t') - V_w(t')\right]. \quad \text{(A3)}$$

Note that the second term on the left-hand side of Eqn A2 is made necessary by the fact that the engulfed mass loses momentum and energy to each new slug 'dM_w' entering the cavity during time increment dt [this term arises from a more fundamental definition of momentum change, $d(V_w M_w)/dt = M_w dV_w/dt + V_w dM_w/dt$, where $dM_w/dt = \rho_w A_c(t)(V_c - V_w)$]. Ψ is a proportionality constant whose meaning is discussed at the end of this section.

In both Eqns A1 and A3, the function $A_c(t)$ is the instantaneous (vertical) cross-section mouth area measured just below the TMJ [see fig. 5 in Potvin et al. (Potvin et al., 2009)]. It is calculated as the surface area of a half-ellipse, which is a good approximation of the mandible and cavity shapes observed in the field (Goldbogen et al., 2010):

$$A_c(t) = \frac{1}{2}\pi \frac{w_{head}}{2}\left[0.98 L_{jaw} \sin\theta_{gape}(t)\right]. \quad \text{(A4)}$$

The semi-minor and major radii of this elliptical area are defined by the half-width of the head ($w_{head}/2$) and (axially) projected length of the (distended) jaw [$0.98 L_{jaw}\sin\theta_{gape}(t)$], with $\theta_{gape}(t)$ corresponding to the gape angle (Table A1 lists representative values of these body dimensions). The species-specific '0.98' factor is needed to insure a good match with the value of $A_c(t)$ estimated from morphology for an 'average' 25 m adult fin whale. Such a factor will be assumed to be independent of body length. In this version of the BLFM, $\theta_{gape}(t)$ is a known function further discussed in Potvin et al. (Potvin et al., 2010).

Strictly speaking, Eqn A3 measures the mass engulfed post-TMJ only (i.e. $M_w = M_w^{post\text{-}TMJ}$), as it uses the mouth cross-sectional area directly below the TMJ to measure the flux of fluid entering the cavity. Using $M_w^{post\text{-}TMJ}$ is warranted during the mouth opening stage of engulfment because it is functionally identical to the total mass

Table A1. Body dimensions and energy estimates of the simulated blue whales

L_{body} (m)	L_0 (m)	L_{jaw} (m)	w_{head} (m)	A_{body} (m^2)
22.1	12.58	4.17	2.53	6
25.2	14.71	5.02	2.96	10
27.0	15.98	5.54	3.22	12

A_{body}, cross-section area of the body; L_0, length of the ventral groove blubber; L_{body}, length of the body; L_{jaw}, length of the lateral projection of the jaw; w_{head}, width of the head.

being engulfed during that time. However, the equation clearly neglects the (smaller) mass accumulating in the buccal cavity anterior to the TMJ (ant-TMJ) during the mouth closure stage. The extent of this omission can be gauged with the results of a recent study of the volumetric capacities of large rorquals (Goldbogen et al., 2010), which suggests that $M_{\mathrm{w}}^{\text{ant-TMJ}}/M_{\mathrm{w}}^{\text{post-TMJ}}=L_{\mathrm{jaw}}/(L_0-L_{\mathrm{jaw}})$, where L_0 corresponds to the entire length of the VGB (from the anterior end of the mandible to the umbilicus) and L_{jaw} is the length of the lateral projection of the jaw. Given the data in Table A1, this mass ratio equals ~50% for all three sizes, thus yielding an approximately 30% [(0.5/1.5)×100] underestimate of the total mass captured by the end of mouth closure. From an energetics point of view, omitting the effects of the mass accumulating ant-TMJ yields an error of approximately 20% in the calculation the kinetic energy imparted to the engulfed mass. This is evident from the following (simplified) model where: (1) half of the mass accumulating post-TMJ has been accelerated from rest to speeds of approximately 3.68 m s^{-1} during the first half of mouth opening (see tag data, Fig. 5), whereas the other half has accelerated to an average speed of ~3.0 m s^{-1} during the second half of the mouth opening stage; and (2) half of the mass accumulating ant-TMJ has been accelerated to speeds of approximately 2.20 m s^{-1} (mean) during the first half of mouth closing, and the other half accelerated to an average speed of ~1.6 m s^{-1} during the second half of mouth closing. The gained kinetic energy (ΔE_{K}) is then calculated as follows:

$$\Delta E_{\mathrm{K}}\big|_{\text{post-TMJ}} \approx \frac{1}{2}\left(M_{\mathrm{w}}^{\text{post-TMJ}}/2\right)_{\text{filled}}\left(3.68^2-0\right) + \frac{1}{2}\left(M_{\mathrm{w}}^{\text{post-TMJ}}/2\right)_{\text{filled}}\left(3.00^2-0\right) \approx 5.63\,(\mathrm{ms}^{-1})^2\left(M_{\mathrm{w}}^{\text{post-TMJ}}\right)_{\text{filled}} \quad \text{(A5)}$$

$$\Delta E_{\mathrm{K}}\big|_{\text{ant-TMJ}} \approx \frac{1}{2}\left(M_{\mathrm{w}}^{\text{post-TMJ}}/4\right)_{\text{filled}}\left(2.20^2-0\right) + \frac{1}{2}\left(M_{\mathrm{w}}^{\text{post-TMJ}}/4\right)_{\text{filled}}\left(1.60^2-0\right) \sim 0.92\ (\mathrm{ms}^{-1})^2\left(M_{\mathrm{w}}^{\text{post-TMJ}}\right)_{\text{filled}}. \quad \text{(A6)}$$

Note that in Eqn A6 we have used $M_{\mathrm{w}}^{\text{ant-TMJ}}/M_{\mathrm{w}}^{\text{post-TMJ}}\approx 1/2$. To the extent that roughly the same distance is being travelled in simulations with and without $M_{\mathrm{w}}^{\text{ant-TMJ}}$, and in a context where T and F_{ext} are much smaller than drag (see Forces relevant to engulfment), underestimating the energetics by 20% means that the total drag ($F_{\mathrm{SD}}+F_{\mathrm{ED}}$) is also underestimated by approximately 20% (J.P., unpublished data).

As the last symbol of the fundamental equations (Eqns A1–A4), the parameter ψ is another improvement to the original BLFM and is used to yield the volume of the filled cavity post-TMJ that is predicted by morphology (Goldbogen et al., 2010), by the time of maximum gape. Given the one-dimensional fluid dynamics invoked

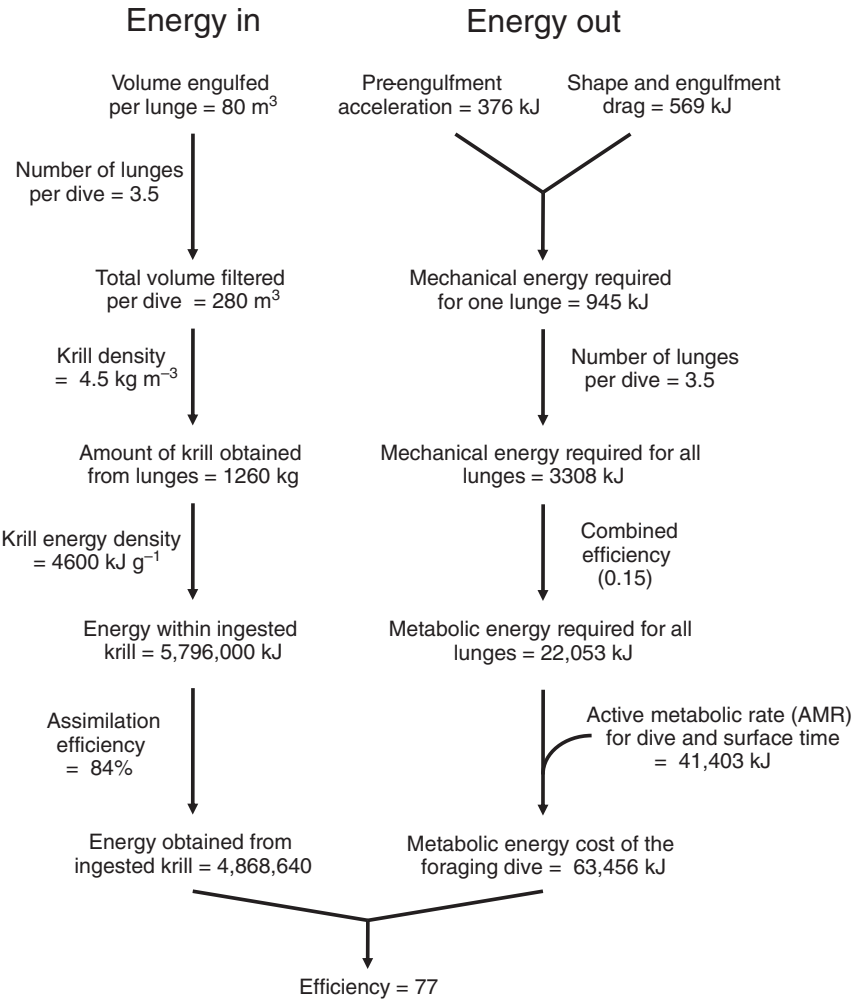

Fig. A1. Energy budget for lunge-feeding efficiency during foraging dives. Example values are given at each step of the calculation for a 25 m blue whale (Table 3). Models from Croll et al. were used to estimate active metabolic rate (AMR) (Croll et al., 2006).

above, where each engulfed slug dM_w passing below the TMJ never changes shape once inside the cavity (post-TMJ), Eqn A3 with ψ=1 effectively yields the volumetric capacity of a 1/4-ellipsoidal wedge (i.e. a wedge with an elliptical cross-section) rather than that of a 1/4-three dimensional ellipsoid, which appears to better approximate the filled buccal cavities seen in the field.

A three-dimensional ellipsoid shape for the fully inflated buccal cavity is a direct consequence of the engulfed slugs of water changing shape after engulfment. This scenario implies that: (1) the fluid dynamics are three-dimensional (rather than just one-dimensional), and (2) the buccal cavity is able to extend sufficiently to accommodate an ellipsoid shape. Setting ψ>1 makes a one-dimensional fluid dynamic scheme appear three-dimensional by effectively increasing the fluid's speed at the entry point into the cavity (i.e. at TMJ-level) to $\psi[V_c(t)–V_w(t)]$ (*via* Eqn A3). Concomitantly, the longitudinal expansion of the buccal cavity (post-TMJ) is modulated at a slower pace, i.e. as determined by a_w and V_w in Eqns A2 and A9 (below). Here, ψ=4/3 given that the volumetric capacity of ellipsoids is greater than that of ellipsoidal wedges by a factor of four-thirds.

Forces relevant to engulfment

Engulfment drag and buccal cavity wall force

The most important force acting on a lunge-feeding whale is the push exerted by the buccal cavity walls onto the engulfed mass (F_{BC}). By action–reaction, such a force gives rise to engulfment drag (i.e. F_{ED} as F_{ED}=F_{BC}), which adds to the so-called shape drag (F_{SD}) being produced by the flow around the whale's body (external drag). Several possible forms for F_{BC} were considered in Potvin et al. (Potvin et al., 2009), including the elastic force provided by the VGB, a hydrodynamic force proportional to the stagnation pressure at the anterior end of the rostrum and the so-called forward shove (see below). As discussed elsewhere (Potvin et al., 2010), VGB elastic forces appear to play only a minor role during lunges. Moreover, only the shove-type force was found to yield velocity temporal profiles that matched the tag data.

In the BLFM, the acceleration of the engulfed water mass (the forward push) is parameterized as follows:

$$F_{BC}^{open/close}(t) = \frac{k_{open/close}}{t_{engulf}^2}\left[\frac{4A_c(t)}{\pi w_{head}}\right]M_w(t)\ . \qquad (A7)$$

The function $F_{BC}^{open}(t)$ and (input) constant k_{open} characterize the mouth-opening stage and F_{BC}^{close} and k_{close} the mouth-closing stage. The basic distance scale for this force is set by the ratio A_c/w_{head}, calculated from Eqn A4, and the morphometrics of the body data (Table A1). By contrast, the time scale of the shove is set by the duration of the engulfment process itself, as calculated from (Potvin et al., 2010):

$$t_{engulf} = 2\Gamma\left(\frac{L_0 - L_{jaw}}{L_{jaw}}\right)\frac{L_{jaw}}{V_c(0)}\ . \qquad (A8)$$

Here Γ is a constant estimated at ~6/5 that is weakly dependent on body length (Potvin et al., 2010). Using again the body dimension data of Table A1 yields $2\Gamma(L_0–L_{jaw})/L_{jaw}$=4.66±0.15. The value of 4.66 was used in the simulations for all three body dimensions. As a result, Eqn A8 yielded an engulfment time of 6.59 s for the 25 m whale simulation shown in Fig. 5, where $V_c(0)$=3.68 m s^{-1}.

The so-called reaction constants k_{open} and k_{close} directly determine how 'hard' the engulfed mass is being pushed forward: too hard of a push and the mass exits the cavity as $V_c(t)$<$V_w(t)$ (i.e. cavity draining); too weak of a push and the cavity post-TMJ fills up too soon, i.e. prior to maximum gape. The buccal cavity is completely filled when the engulfed water mass reaches the posterior end of the buccal cavity, an event occurring when:

$$X_c(t) - X_w(t) \equiv \int_0^t dt'\left[V_c(t') - V_w(t')\right] = L_0 - L_{jaw}\ , \qquad (A9)$$

where X_c and X_w are the distances traveled by points located at the TMJ and aft-end of the engulfed mass, respectively, and t' is time, used here as an integration variable.

In between these two limits there is a continuum of values that generally yield partial or incomplete filling of the buccal cavity relative to the maximum capacity predicted by morphology. During the mouth opening stage, only the lower value of the range for k_{open} yields the maximum volumetric capacity (post-TMJ) that is limited by morphology (Goldbogen et al., 2010). Typically, optimal k_{open} is determined after several trial simulations (i.e. prior to an 'official' run) and yielded: k_{open}/t_{engulf}^2=0.15 to 0.26 s^{-2} (27 m whale), 0.18 to 0.34 s^{-2} (25 m) and 0.28 to 0.40 s^{-2} (22 m) [the specific value depended on $V_c(0)$ and the shape drag coefficients discussed below]. As discussed recently (Potvin et al., 2010), the muscle within the VGB must relax somewhat to allow the closing of the mouth following maximum gape, an action that must substantially diminish the forward push of the engulfed mass. For this reason, our simulations were carried out with k_{close}=0.

Shape drag

The drag associated with the changing shape of a lunge-feeding whale and the external flows that result can be parameterized by this general formula:

$$F_{SD}(t) \equiv C(t)S(t)\left(\frac{1}{2}\rho_w V_c^2(t)\right)\ . \qquad (A10)$$

The function $C(t)S(t)$ corresponds to the instant drag area of the shape generating the drag. This time-dependent function has dimensions of surface area and represents the combined effects of the accelerating and decelerating external flows taking place around the whale (i.e. the so-called added mass), as well as the effects of wake growth and wake turbulence that are generated during the lunge (Potvin et al., 2009). Here one uses:

$$C(t)S(t)|_{mouthopening} = C_{Dopen}A_c(t) + C_{Dbody}A_{body}\ , \qquad (A11)$$

$$C(t)S(t)|_{mouthclosing} = C_{Dclose}A_c^{max} + C_{Dbody}A_{body}\ . \qquad (A12)$$

The parameter A_{body} is the (known) cross-section of the body in a closed-mouth, empty-cavity configuration (Goldbogen et al., 2009b), here equal to 10 m^2 in the case of the 25 m blue whale (Table A1); C_{Dbody} is the corresponding drag coefficient, set to 0.05 from a previous hydrodynamic study on fin whale locomotion (Bose and Lien, 1989) [note: these authors quote C_{Dbody}=0.0026, which is based instead on a 131 m^2 total body surface area of a fin whale, rather than its cross-section (7 m^2)].

The known instantaneous mouth area $A_c(t)$ (Eqn A4) and maximum mouth area A_c^{max} (Eqn A4, with θ_{gape}^{gape}=80 deg) were assigned the following drag coefficients: C_{Dopen}≈0.33 and C_{Dclose}≈1.2 to 2.0. These variations in the drag function $C(t)$ between the mouth-opening and mouth-closing stages have a very coarse time dependence, but one that reflects an overall increase in drag

coefficient owing to the unsteady nature of the flow outside and right behind the buccal cavity.

Fluking thrust and buoyancy-reduced weight

Calculating the relevant values for fluking thrust (T) and buoyancy-reduced weight (F_{ext}) during engulfment is a tentative exercise given that these forces have never been experimentally quantified to an extent that is useful for simulation studies. However, this may be a moot point because the estimates that follow indicate that T and F_{ext} may be very small relative to engulfment drag (F_{ED}), and furthermore, that they could cancel each other by virtue of having similar magnitude. Accordingly, the sum $T+F_{ext}$ in Eqn A1 was set to zero in the simulations.

The buoyancy-reduced weight, defined as $F_{ext}=(F_B-W_c)\sin\varphi_{glide}$, with F_B, W_c and φ_{glide} corresponding to a whale's buoyancy, weight and glide angle during descent, respectively, can be estimated from the drag properties of the body during the constant-speed phase of a gliding descent to the bottom (Goldbogen et al., 2006). At terminal velocity near the end of a descent (a state of dynamic equilibrium), one has $(F_B-W_c)\sin\varphi_{glide}=F_{SD}$ in the absence of any significant fluking thrust (of which there is none according to the tag data). Thus, from Eqn A10 with $C(t)S(t)=C_{Dbody}A_{body}$ ($=10\ m^2\times0.05$) and $V_c=4.0\pm0.5\ m\ s^{-1}$ (obtained from the tag data of eight whales), one calculates $F_{ext}=(F_B-W_c)\sin\varphi_{glide}\approx4100\ N$.

Fluking thrust during engulfment (T_E) will be estimated as a fraction of the thrust generated during the 'uphill' portion of the pre-engulfment phase (T_{PE}) (Fig. 2), where the whale accelerates towards the krill patch from below for approximately 3 s. Estimating T_{PE} will be carried out with the integral version of Newton's law of motion, also known as the momentum-impulse (MI) theorem (French, 1971). Along the uphill and straight trajectory assumed to be taken here, the MI theorem results in the time-averaged forces being given by the following:

$$M_c\Delta V_c=(\langle T_{PE}\rangle-\langle F_{SD}\rangle-\langle F_{ext}\rangle)t_{uphill}\,, \tag{A13}$$

where t_{uphill} is the duration of that portion of the pre-engulfment phase. With $t_{uphill}\approx3$ s, $\Delta V_c\approx3.7$–$2.0\ m\ s^{-1}$ (Fig. 2), $M_c=96{,}568$ kg (Table 2, 25 m whale) and $F_{SD}\approx F_{ext}\approx4100$ N (previous paragraph), one obtains $T_{PE}\approx54{,}722+8200\ N=62{,}922$ N. Relating the value of T_E to that of T_{PE} follows from the ratio of peak fluking acceleration $a^{E}_{fluke}/a^{PE}_{fluke}$ shown in Fig. 2, which generally varies between 0.2/2.0 and 0.5/2.0 in the three lunges shown in Fig. 2. To the extent that the (tangential) acceleration of the flukes reflects that of the fluid being pushed rearward, and that the fluid mass being pushed by the flukes is similar during both engulfment and pre-engulfment, one would expect the ratio T_E/T_{PE} to have similar values, within one order of magnitude. Thus, we predict T_E to be in the range of 6292 to 15,731 N, which is significantly smaller than the peak engulfment drag being generated ($F^{peak}_{ED}>50$ kN).

Water-to-water drag

The last force of relevance to the BLFM is the hydrodynamic force F_{ww} applied on the engulfed slugs in the process of re-exiting the mouth during mouth closure ($F_{ww}=0$ during mouth opening). These forces arise from the interaction of those slugs with the rest of the ocean that surrounds the whale. The BLFM represents this interaction with the drag equation (Eqn A10), where $C(t)S(t)=0.1A_c(t)$ when $V_c(t)>V_w(t)$ and $C(t)S(t)=0$ when $V_c(t)\leq V_w(t)$. This is a rather crude approach to a complicated hydrodynamic phenomenon. An improved representation for F_{ww}, as implemented along with an explicit accounting of the mass captured anteriorily to the TMJ, is currently being developed and tested.

Input parameters

Our simulations were obtained from the numerical integration of the equations of motion using the simple Euler–Cromer algorithm (Gould and Tobochnik, 1996). Although usually unsuitable for most multi-temporal scale simulations, Euler's method is accurate for the problem at hand given that the two time scales operating here, namely that of the mouth cross-section area [$A_c(t)$] and that of shape drag, are of the same order of magnitude, i.e. 10^0–10^1 s (Potvin et al., 2009). As a further check, several simulations were performed at a shorter time increment ($dt=0.001$ s) in addition to the increment of $dt=0.01$ s used for all simulations, and were verified to yield identical results.

The BLFM incorporates a large number of input parameters corresponding to the dimensions of the body, namely L_{body}, L_0, w_{head}, L_{jaw}, M_c and A_{body} (Table 2 and Table A1). Other parameters used here included the density of seawater ($\rho_w=1025\ kg\ m^{-3}$), maximum gape angle ($\theta^{out}_{gape}=80$ deg$=1.39$ rad), and initial speed of engulfed water [$V_w(0)=0$]. Most importantly, initial speeds of 3.1, 3.68 and 4.10 m s^{-1} were considered to gauge the variability with regards to the sensitivity of the results to initial speed. The values of the parameters related to the forces of relevance were listed in the previous section.

Simple veracity check

We checked the veracity of our simulations using the following simple but correct energy relationships (Potvin et al., 2010). Along straight-line trajectories, horizontal or angled, over which F_{ext} and T are negligible, a whale's drag energy losses (ΔQ_{drag}) during engulfment can be assessed *via* the integral over travel distance for the equation of motion (Eqn A1), namely:

$$\frac{\Delta Q_{drag}}{M_c}=\int_0^{X_c(t_{engulf})}\frac{\left|F_{ED}+F_{SD}\right|}{M_c}\mathrm{d}x=\int_0^{X_c(t_{engulf})}\frac{M_c\left|a_c(t)\right|}{M_c}\mathrm{d}x$$
$$=\frac{V_c^2(0)}{2}\left(1-\frac{V_c^2(t_{engulf})}{V_c^2(0)}\right). \tag{A14}$$

Again, the engulfment time t_{engulf} is computed from Eqn A8. The derivation of the mean rate of energy loss [$P_{drag}(t)$] follows a similar reasoning and from the fact that $P_{drag}(t)$ is the time derivative of $Q_{drag}(t)$. Averaging $P_{drag}(t)$ over the duration of engulfment yields exactly:

$$\frac{\left\langle P_{drag}\right\rangle}{M_c}\equiv\frac{1}{t_{engulf}}\int_0^{t_{engulf}}\frac{\mathrm{d}}{\mathrm{d}t}\left(\frac{Q_{drag}}{M_c}\right)\mathrm{d}t$$
$$=\frac{1}{M_c t_{engulf}}\int_0^{t_{engulf}}\mathrm{d}Q_{drag}=\frac{\Delta Q_{drag}}{M_c t_{engulf}}\,. \tag{A15}$$

Given the dependence of ΔQ_{drag} and P_{drag} on the speed $V_c(t_{engulf})$ at the end of engulfment (and prior to purging the engulfed water mass past the baleen), this veracity check requires knowing (or approximating) the scaling of $V_c(t_{engulf})$ as well. This is done from the fact that the speed decrement over engulfment time is (exactly) equal to the time-averaged deceleration:

$$V_c(0)-V_c(t_{engulf})=\left\langle a_c\right\rangle t_{engulf}$$
$$\sim\frac{L_0}{\left(t_{engulf}\right)^2}t_{engulf}=\frac{L_0}{2\Gamma\left(L_0-L_{jaw}\right)}V_c(0)\,. \tag{A16}$$

The second line of the equation approximates $\langle|a_c|\rangle$ as the ratio of a travel distance scale (L_0) over the square of a characteristic time (t_{engulf}^2) and involves Eqn A8 in the last step. The use of L_0 as a typical distance scale can be argued from constant-acceleration kinematics, where $t_{engulf}^2\langle a_c\rangle=2(d-V_c(0)t_{engulf})$; this result is used along with Eqn A8 while approximating L_0 as $L_0\approx d$ (i.e. the actual travel distance, which is good only for large adults), approximating L_{jaw} as $L_{jaw}\approx 1/3L_0$ (as suggested by morphology) and setting $1.2\approx 1.0$. The body size data of Table A1 thus show that the ratio $[V_c(0)-V_c(t_{engulf})]/V_c(0)$ is ~0.64 [or $V_c(t_{engulf})\approx 0.36V_c(0)$] for the three sizes of blue whales considered here, which is in overall agreement with the simulations (i.e. within $\pm 0.15\,m\,s^{-1}$).

Using Eqns A14 and A16 yields the following energy losses due to drag, in the case of a 25 m whale moving at $V_c(0)=3.68\,m\,s^{-1}$ at the beginning of engulfment: $\Delta Q_{drag}=365{,}373$ J (22 m whale), 575,415 J (25 m) and 730,561 J (27 m). These values compare well with the simulation values discussed in the text. The mass-specific rate of energy loss (at the same initial speed) comes from Eqns A15 and A16: $P_{drag}/M_c=1.12\,W\,kg^{-1}$ (22 m whale), $0.95\,W\,kg^{-1}$ (25 m) and $0.88\,W\,kg^{-1}$ (27 m), which again match those of the simulations.

APPENDIX 2. EXAMPLE ENERGY BUDGET FOR LUNGE-FEEDING EFFICIENCY DURING FORAGING DIVES

We estimated the energetic efficiency of blue whale foraging dives by accounting for the energy obtained from ingested prey and the energy expended during diving and lunge feeding (Fig. A1). The energy input accounted for assimilation efficiency and variation in krill density (Table 3). The energy expenditures included the mechanical energy required to lunge (Appendix 1), the combined efficiency of converting metabolic energy into mechanical energy (0.15) and AMR during diving and post-dive recovery time.

LIST OF ABBREVIATIONS

A_{body}	cross-section area of the body (closed-mouth, empty-cavity configuration)
a_c	acceleration of an empty whale
A_c	instantaneous (vertical) cross-section mouth area
a_{fluke}	fluking acceleration
A_{mouth}	mouth area
AMR	active metabolic rate
a_w	acceleration of engulfed water
BLFM	basic lunge-feeding model
BMR	basal metabolic rate
d	travel distance
E_K	kinetic energy
F_B	buoyancy
F_{BC}	buccal cavity wall force
F_{ED}	engulfment drag force
F_{ext}	whale's weight minus buoyancy, projected along the direction of motion
FMR	field metabolic rate
F_{SD}	shape drag force
F_{ww}	water-to-water drag force
k_{close}	reaction constant used in Eqn A7 to calculate the cavity wall force during mouth closing
k_{open}	reaction constant used in Eqn A7 to calculate the cavity wall force during mouth opening
L_0	length of the VGB (from the anterior end of the mandible to the umbilicus)
L_{body}	body length
L_{jaw}	length of the jaw
M_{body}	body mass
M_c	mass of an empty whale
M_w	mass of engulfed water
P_{drag}	Energy loss
Q_{drag}	whale drag energy
t	time
T	fluking thrust
TADL	theoretical aerobic dive limit
T_E	engulfment fluking thrust
t_{engulf}	engulfment time
TMJ	temporomandibular joint
T_{PE}	pre-engulfment fluking thrust
V_c	whale speed
VGB	ventral groove blubber
V_w	engulfed water speed
W	whale weight
Γ	proportionality constant used in Eqn A8, ~6/5
θ_{gape}	gape angle
ρ_w	density of seawater
φ_{glide}	glide angle during descent
ψ	proportionality constant used in Eqn A3, =4/3
ω_{head}	width of the head

ACKNOWLEDGEMENTS

Funding was provided by the United States Navy (SERDP Robert Holst, CNO-N45 Frank Stone, ONR Bob Gisiner) and NSERC to R.E.S. We thank J. A. Hildebrand for financial and logistical support related to the digital tags and tagging operations. J.A.G. was supported by the Scripps Institution of Oceanography Postdoctoral Fellowship Program. N.D.P. is supported by funds from the University of California Museum of Paleontology Remington Kellogg Fund, an NSF Graduate Research Fellowship, an NSERC Postdoctoral Research Fellowship and the Smithsonian Institution. We thank Donald Croll and Kelly Newton for providing the hydroacoustic prey map used in Fig. 2.

REFERENCES

Acevedo-Gutierrez, A., Croll, D. A. and Tershy, B. R. (2002). High feeding costs limit dive time in the largest whales. *J. Exp. Biol.* **205**, 1747-1753.

Ahlborn, B. K. (2004). *Zoological Physics*. Berlin: Springer-Verlag.

Alexander, R. M. (1998). All-time giants: the largest animals and their problems. *Palaeontology* **41**, 1231-1245.

Bose, N. and Lien, J. (1989). Propulsion of a fin whale (*Balaenoptera physalus*) – why the fin whale is a fast swimmer. *Proc. R. Soc. Lond. B Biol. Sci.* **237**, 175-200.

Boyd, I. (2002). Marine mammal energetics. In *Marine Mammal Biology: an Evolutionary Approach* (ed. A. Hoelzel), pp. 247-277. Oxford, UK: Blackwell.

Brodie, P. F. (1975). Cetacean energetics, an overview of intraspecific size variation. *Ecology* **56**, 152-161.

Brodie, P. F. (1978). Alternative sampling device for aquatic organisms. *J. Fish. Res. Board Can.* **35**, 901-902.

Brodie, P. F. (1993). Noise generated by the jaw actions of feeding fin whales. *Can. J. Zool.* **71**, 2546-2550.

Brodie, P. F. (2001). Feeding mechanics of rorquals *Balaenoptera* sp. In *Secondary Adaptations of Tetrapods to Life in Water* (ed. J. M. Mazin and V. de Buffrenil), pp. 345-352. Munchen, Germany: Verlag.

Calambokidis, J., Schorr, G. S., Steiger, G. H., Francis, J., Bakhtiari, M., Marshal, G., Oleson, E. M., Gendron, D. and Robertson, K. (2007). Insights into the underwater diving, feeding, and calling behavior of blue whales from a suction-cup-attached video-imaging tag (CRITTERCAM). *Mar. Technol. Soc. J.* **41**, 19-29.

Clapham, P. (2001). Why do baleen whales migrate? A response to Corkeron and Connor. *Mar. Mammal Sci.* **17**, 432-436.

Cooper, L. N., Sedano, N., Johansson, S., May, B., Brown, J. D., Holliday, C. M., Kot, B. W. and Fish, F. E. (2008). Hydrodynamic performance of the minke whale (*Balaenoptera acutorostrata*) flipper. *J. Exp. Biol.* **211**, 1859-1867.

Corkeron, P. J. and Connor, R. C. (1999). Why do baleen whales migrate? *Mar. Mammal Sci.* **15**, 1228-1245.

Cotte, C. and Simard, Y. (2005). Formation of dense krill patches under tidal forcing at whale feeding hot spots in the St Lawrence Estuary. *Mar. Ecol. Prog. Ser.* **288**, 199-210.

Croll, D. A., Tershy, B. R., Hewitt, R. P., Demer, D. A., Fiedler, P. C., Smith, S. E., Armstrong, W., Popp, J. M., Kiekhefer, T., Lopez, V. R. et al. (1998). An integrated approach to the foraging ecology of marine birds and mammals. *Deep Sea Res. Part II-Top. Stud. Oceanogr.* **45**, 1353-1371.

Croll, D. A., Acevedo-Gutierrez, A., Tershy, B. R. and Urban-Ramirez, J. (2001). The diving behavior of blue and fin whales: is dive duration shorter than expected based on oxygen stores? *Com. Biochem. Physiol. A Physiol.* **129**, 797-809.

Croll, D. A., Marinovic, B., Benson, S., Chavez, F. P., Black, N., Ternullo, R. and Tershy, B. R. (2005). From wind to whales: trophic links in a coastal upwelling system. *Mar. Ecol. Prog. Ser.* **289**, 117-130.

Croll, D. A., Kudela, R. and Tershy, B. R. (2006). Ecosystem impact of the decline of large whales in the North Pacific. In *Whales, Whaling and Ocean Ecosystems* (ed. J. A. Estes), pp. 202-214. Berkeley, CA: University of California Press.

Demer, D. A. and Hewitt, R. P. (1995). Bias in acoustic biomass estimates of *Euphausia sperba* due to diel vertical migration. *Deep Sea Res. Part I-Oceanogr. Res. Papers* **42**, 455-475.

Dolphin, W. F. (1987). Prey densities and foraging of humpback whales, *Megaptera novaeangliae*. *Experientia* **43**, 468-471.

Fahlman, A., Svard, C., Rosen, D. A. S., Jones, D. R. and Trites, A. W. (2008a). Metabolic costs of foraging and the management of O_2 and CO_2 stores in Steller sea lions. *J. Exp. Biol.* **211**, 3573-3580.

Fahlman, A., Wilson, R., Svard, C., Rosen, D. A. S. and Trites, A. W. (2008b). Activity and diving metabolism correlate in Steller sea lion *Eumetopias jubatus*. *Aquat. Biol.* **2**, 75-84.
Fiedler, P. C., Reilly, S. B., Hewitt, R. P., Demer, D., Philbrick, V. A., Smith, S., Armstrong, W., Croll, D. A., Tershy, B. R. and Mate, B. R. (1998). Blue whale habitat and prey in the California Channel Islands. *Deep Sea Res. Part II-Top. Stud. Oceanogr.* **45**, 1781-1801.
Fish, F. E. and Rohr, J. J. (1999). Review of dolphin hydrodynamics and swimming performance. In *SPAWARS System Center Technical Report*. San Diego, CA: SSC.
French, A. P. (1971). *Newtonian Mechanics*. New York: WW Norton and Company, Inc.
Friedlaender, A. S., Hazen, E. L., Nowacek, D. P., Halpin, P. N., Ware, C., Weinrich, M. T., Hurst, T. and Wiley, D. (2009). Diel changes in humpback whale *Megaptera novaeangliae* feeding behavior in response to sand lance *Ammodytes* spp. behavior and distribution. *Mar. Ecol. Prog. Ser.* **395**, 91-100.
Friedman, M., Shimada, K., Martin, L. D., Everhart, M. J., Liston, J., Maltese, A. and Triebold, M. (2010). 100-million-year dynasty of giant planktivorous bony fishes in the mesozoic seas. *Science* **327**, 990-993.
Goldbogen, J. A. (2010). The ultimate mouthful: lunge feeding in rorqual whales. *Am. Sci.* **98**, 124-131.
Goldbogen, J. A., Calambokidis, J., Shadwick, R. E., Oleson, E. M., McDonald, M. A. and Hildebrand, J. A. (2006). Kinematics of foraging dives and lunge-feeding in fin whales. *J. Exp. Biol.* **209**, 1231-1244.
Goldbogen, J. A., Pyenson, N. D. and Shadwick, R. E. (2007). Big gulps require high drag for fin whale lunge feeding. *Mar. Ecol. Prog. Ser.* **349**, 289-301.
Goldbogen, J. A., Calambokidis, J., Croll, D., Harvey, J., Newton, K., Oleson, E., Schorr, G. and Shadwick, R. E. (2008). Foraging behavior of humpback whales: kinematic and respiratory patterns suggest a high cost for a lunge. *J. Exp. Biol.* **211**, 3712-3719.
Goldbogen, J. A., Potvin, J. and Shadwick, R. E. (2010). Skull and buccal cavity allometry increase mass-specific engulfment capacity in fin whales. *Proc. R. Soc. Lond. B Biol. Sci.* **277**, 861-868.
Gould, H. and Tobochnik, J. (1996). *An Introduction to Computer Simulation Methods*. New York: Addison-Wesley.
Hamner, W. M. (1984). Aspects of schooling in *Euphasia superba*. *J. Crust. Biol.* **4**, 67-74.
Hamner, W. M., Hamner, P. P., Strand, S. W. and Gilmer, R. W. (1983). Behavior of Antarctic krill, *Euphausia superba*: chemoreception, feeding, schooling, and molting. *Science* **220**, 433-435.
Herwig, R. P., Staley, J. T., Nerini, M. K. and Braham, H. W. (1984). Baleen whales-preliminary evidence for forestomach microbial fermentation. *Appl. Environ. Microbiol.* **47**, 421-423.
Hewitt, R. P. and Demer, D. A. (2000). The use of acoustic sampling to estimate the dispersion and abundance of euphausiids, with an emphasis on Antarctic krill, *Euphausia superba*. *Fish. Res.* **47**, 215-229.
Hovenkamp, S. (1989). Avoidance of nets by *Euphausia pacifica* in Dabob Bay. *J. Plankt. Res.* **11**, 907-924.
Lambertsen, R. H. (1983). Internal mechanism of rorqual feeding. *J. Mammal.* **64**, 76-88.
Lavigne, D. M., Innes, S., Worthy, G. A. J. and Edwards, E. F. (1990). Lower critical temperatures of blue whales, *Balaenoptera musculus*. *J. Theor. Biol.* **144**, 249-257.
Lockyer, C. (1976). Body weights of some species of large whales. *ICES J. Mar. Sci.* **36**, 259-273.
Lockyer, C. (1981). Growth and energy budgets of large baleen whales from the Southern Hemisphere. *FAO Fish. Ser.* **5**, 379-487.
Lockyer, C. (1986). Body fat condition in Northeast Atlantic fin whales, *Balaenoptera physalus*, and its relationship with reproduction and food resource. *Can. J. Fish. Aquat. Sci.* **43**, 142-147.
Lockyer, C. (2007). All creatures great and smaller: a study in cetacean life history energetics. *J. Mar. Biol. Assoc. UK* **87**, 1035-1045.
Mackintosh, N. A. and Wheeler, J. F. G. (1929). Southern blue and fin whales. *Discov. Rep.* **1**, 257-540.
Nicol, S. (1986). Shape, size and density of daytime surface swarms of the euphausiid *Meganyctiphanes norvegica* in the Bay of Fundy. *J. Plankt. Res.* **8**, 29-39.
Ogawa, T. and Shida, T. (1950). On the sensory tubercles of lips and oral cavity in the sei and fin whale. *Sci. Rep. Whales Res. Inst.* **3**, 1-16.
Oleson, E. M., Calambokidis, J., Burgess, W. C., McDonald, M. A., LeDuc, C. A. and Hildebrand, J. A. (2007). Behavioral context of call production by eastern North Pacific blue whales. *Mar. Ecol. Prog. Ser.* **330**, 269-284.
Olsen, M. A., Blix, A. S., Utsi, T. H. A., Sormo, W. and Mathiesen, S. D. (2000). Chitinolytic bacteria in the minke whale forestomach. *Can. J. Microbiol.* **46**, 85-94.
Orton, L. S. and Brodie, P. F. (1987). Engulfing mechanics of fin whales. *Can. J. Zool.* **65**, 2898-2907.
Panigada, S., Zanardelli, M., Canese, S. and Jahoda, M. (1999). How deep can baleen whales dive? *Mar. Ecol. Prog. Ser.* **187**, 309-311.
Panigada, S., Pesante, G., Zanardelli, M. and Oehen, S. (2003). Day and night-time diving behavior of fin whales in the western Ligurian Sea. *Proceedings Oceans 2003* **1**, 466-471.
Potvin, J., Goldbogen, J. A. and Shadwick, R. E. (2009). Passive versus active engulfment: verdict from trajectory simulations of lunge-feeding fin whales *Balaenoptera physalus*. *J. R. Soc. Interface* **6**, 1005-1025.
Potvin, J., Goldbogen, J. A. and Shadwick, R. E. (2010). Scaling of lunge feeding in rorqual whales: an integrated model of engulfment duration. *J. Theor. Biol.* **267**, 437-453.
Rasmussen, K., Palacios, D. M., Calambokidis, J., Saborio, M. T., Dalla Rosa, L., Secchi, E. R., Steiger, G. H., Allen, J. M. and Stone, G. S. (2007). Southern Hemisphere humpback whales wintering off Central America: insights from water temperature into the longest mammalian migration. *Biol. Lett.* **3**, 302-305.
Rosen, D. A. S., Winship, A. J. and Hoopes, L. A. (2007). Thermal and digestive constraints to foraging behaviour in marine mammals. *Philos. Trans. R. Soc. Lond. B Biol. Sci.* **362**, 2151-2168.
Ryg, M., Lydersen, C., Knutsen, L. O., Bjorge, A., Smith, T. G. and Oritsland, N. A. (1993). Scaling of insulation in seals and whales. *J. Zool.* **230**, 193-206.
Sanderson, S. L. and Wassersug, R. (1993). Convergent and alternative designs for vertebrate suspension feeding. In *The Skull: Functional and Evolutionary Mechanisms*, Vol. 3 (ed. J. Hanken and B. K. Hall), pp. 37-112. Chicago, IL: University of Chicago Press.
Sato, K., Charrassin, J. B., Bost, C. A. and Naito, Y. (2004). Why do macaroni penguins choose shallow body angles that result in longer descent and ascent durations? *J. Exp. Biol.* **207**, 4057-4065.
Scholander, P. F. (1940). Experimental investigations on the respiratory function in diving mammals and birds. *Hvalredets Skrifter* **22**, 1-131.
Simard, Y. and Lavoie, D. (1999). The rich krill aggregation of the Saguenay-St Lawrence Marine Park: hydroacoustic and geostatistical biomass estimates, structure, variability, and significance for whales. *Can. J. Fish. Aquat. Sci.* **56**, 1182-1197.
Simard, Y. and Sourisseau, M. (2009). Diel changes in acoustic and catch estimates of krill biomass. *ICES J. Mar. Sci.* **66**, 1318-1325.
Slijper, E. J. (1979). *Whales*. London: Cornell University Press.
Smith, A. H. and Pace, N. (1971). Differential component and organ size relationship among whales. *Environ. Physiol.* **1**, 122-136.
Snyder, G. K. (1983). Respiratory adaptations in diving mammals. *Respir. Physiol.* **54**, 269-294.
Soto, N. A., Johnson, M. P., Madsen, P. T., Diaz, F., Dominguez, I., Brito, A. and Tyack, P. (2008). Cheetahs of the deep sea: deep foraging sprints in short-finned pilot whales off Tenerife (Canary Islands). *J. Anim. Ecol.* **77**, 936-947.
Sourisseau, M., Simard, Y. and Saucier, F. J. (2008). Krill diel vertical migration fine dynamics, nocturnal overturns, and their roles for aggregation in stratified flows. *Can. J. Fish. Aquat. Sci.* **65**, 574-587.
Stimpert, A. K., Wiley, D. N., Au, W. W. L., Johnson, M. P. and Arsenault, R. (2007). 'Megapclicks': acoustic click trains and buzzes produced during night-time foraging of humpback whales (Megaptera novaeangliae). *Biol. Lett.* **3**, 467-470.
Ware, C., Friedlaender, A. S. and Nowacek, D. P. (2010). Shallow and deep lunge feeding of humpback whales in fjords of the West Antarctic Peninsula. *Mar. Mammal Sci.* (in press).
Watts, P., Hansen, S. and Lavigne, D. M. (1993). Models of heat loss by marine mammals: thermoregulation below the zone of irrelevance. *J. Theor. Biol.* **163**, 505-525.
Werth, A. J. (2000). Feeding in marine mammals. In *Feeding: Form, Function and Evolution in Tetrapod Vertebrates* (ed. K. Schwenk), pp. 475-514. New York, NY: Academic Press.
White, C. R., Blackburn, T. M. and Seymour, R. S. (2009). Phylogenetically informed analysis of the allometry of mammalian metabolic rate supports niether geometric nor quarter-power scaling. *Evolution* **63**, 2658-2667.
Williams, T. M. (1999). The evolution of cost efficient swimming in marine mammals: limits to energetic optimization. *Philos. Trans. R. Soc. Lond. Ser. B Biol. Sci.* **354**, 193-201.
Williams, T. M. (2006). Physiological and ecological consequences of extreme body size in whales. In *Whales, Whaling, and Ocean Ecosystems* (ed. J. A. Estes, D. P. DeMaster, D. F. Doak, T. M. Williams and R. L. Brownell), pp. 191-201. Berkeley, CA: University of California Press.
Williams, T. M. and Yeates, L. (2004). The energetics of foraging in large mammals: a comparison of marine and terrestrial predators. *Int. Congr. Ser.* **1275**, 351-358.
Williams, T. M., Haun, J. E. and Friedl, W. A. (1999). The diving physiology of bottlenose dolphins (*Tursiops truncatus*) – I. Balancing the demands of exercise for energy conservation at depth. *J. Exp. Biol.* **202**, 2739-2748.
Williams, T. M., Davis, R. W., Fuiman, L. A., Francis, J., Le Boeuf, B. L., Horning, M., Calambokidis, J. and Croll, D. A. (2000). Sink or swim: strategies for cost-efficient diving by marine mammals. *Science* **288**, 133-136.
Williams, T. M., Haun, J., Davis, R. W., Fuiman, L. A. and Kohin, S. (2001). A killer appetite: metabolic consequences of carnivory in marine mammals. *Comp. Biochem. Physiol. A Mol. Integr. Physiol.* **129**, 785-796.
Williams, T. M., Fuiman, L. A., Horning, M. and Davis, R. W. (2004). The cost of foraging by a marine predator, the Weddell seal *Leptonychotes weddellii*: pricing by the stroke. *J. Exp. Biol.* **207**, 973-982.
Williamson, G. R. (1972). True body shape of rorqual whales. *J. Zool.* **167**, 277-286.